

8 Experimental and numerical investigation of an interlocking system out of osteomorphic cast glass components

The previous chapter concluded that blocks following an osteomorphic geometry are the most promising in respect to the principles of interlocking and glass casting. Moreover, interlayers of the polyurethane (PU) family are considered the most suitable for a building application, without compromising the transparency of the resulting structure. Based on these findings, this chapter aims at investigating the structural behaviour of an interlocking assembly employing osteomorphic blocks and PU as an interlayer. Initially, experimental research is conducted in different PU interlayers available in the market, aiming on finding one that fulfils the established design criteria and mechanical properties, as discussed in chapter 7.6. Different readily available two-component PU interlayers, with a Shore Hardness ranging between 60A – 80A, are cast to follow the osteomorphic interlocking geometry and are tested under static compressive load between two half osteomorphic kiln-cast glass blocks in series of 3 specimens and in 2 different thicknesses (3mm and 6mm). The results suggest that the tearing strength of the interlayer is as important as its Shore Hardness; whereas the geometry of the interlocking form can further influence the overall resistance of the assembly against tearing. They also highlight that insufficient contact (mismatch) of the interlayer with the glass blocks, due to dimensional deviations, can lead to the eventual failure of the assembly even under static load due to peak stresses that are further increased by the lateral stresses occurring due to the creep of the interlayer. From the examined interlayers, PU with a shore hardness between 70A – 80A, are considered as the most suitable for the further experimental validation of the assembly. Following, to investigate the influence of the interlocking mechanism to the structural behaviour of the proposed

system, series of assemblies of osteomorphic blocks with different amplitudes, namely 10, 15 and 20 mm, interweaved with 6 mm thick 70A PU interlayers are tested in out-of-plane shear. The results indicate that blocks with higher amplitudes are stiffer and fail at higher loads and less total deformation. But they are also more prone to dimensional tolerances and eccentricity of the construction. This indicates that a geometry with multiple interlocking mechanisms may be more favourable for the self-alignment of such an assembly. Moreover, all specimens presented visible deformation prior to failure. The pseudo-ductile performance of the assembly and its ability to prevent crack propagation are key-aspects for engineering a safe glass structure. It should be noted that the kiln-cast laboratory fabrication of the examined glass blocks and the use of disposable moulds has resulted in significantly lower dimensional accuracy compared to blocks that would be industrially fabricated using high precision moulds and hot-pouring. These significant dimensional deviations have negatively influenced the behaviour of the assemblies, and therefore, the derived data should be considered only qualitative – it is expected that industrially made blocks will present a considerably improved interlocking behaviour.

Thus, to further explore the influence of the most crucial geometrical aspects of the interlocking mechanism, namely the height and amplitude of the glass components, to the overall structural performance under shear a numerical model⁶⁵ is made. In accordance with the output of the experimental validation, here an osteomorphic block with multiple locks is tested, considering a 4 mm thick 70A PU interlayer. The results of the numerical model indicate that bricks of reduced height are more susceptible to failure by bending, whereas with taller brick variants shear lock failure is more critical. It is also confirmed that an increased amplitude of the interlock can be beneficial as it leads to an increased shear capacity and lower uplifting effects. It is also shown that specimens with increased height reach the failure stress limit with considerably smaller deformations, thus, requiring a higher manufacturing precision.

⁶⁵ The numerical model presented in this chapter is part of the MSc Thesis: Jacobs, E.A.M., Structural consolidation of historic monuments by interlocking cast glass components. TU Delft, 2017.(Jacobs 2017)

Credits

Research partly conducted in collaboration with

- Telesilla Bristogianni – *experimental testing*,
Faculty of Civil Engineering & Geosciences, TU Delft
- Erwin Jacobs – *development and validation of numerical model*,
Faculty of Civil Engineering & Geosciences, TU Delft

Technical support and assistance in prototype manufacturing

- Kees Baardolf,
Stevin II Laboratory, Faculty of Civil Engineering & Geosciences, TU Delft
- Tommaso Venturini,
Faculty of Civil Engineering & Geosciences, TU Delft
- Rong Yu,
Faculty of Civil Engineering & Geosciences, TU Delft

Manufacturing Facilities

- Stevin II Laboratory,
Faculty of Civil Engineering & Geosciences, TU Delft

Research Supervisors

- Rob Nijssse,
Faculty of Civil Engineering & Geosciences, TU Delft
- Fred A. Veer,
Faculty of Architecture & the Built Environment, TU Delft

The research work presented in this chapter has been partly funded by a 4TU.bouw Lighthouse grant for the project Re³ Glass

8.1 Introduction

In the previous chapter a novel structural system employing interlocking cast glass blocks was presented. The proposed system offers several engineering advantages such as an inherent redundancy and resistance to crack propagation, as well as reversibility. To achieve a circular system and at the same time obtain a homogeneous stress distribution the use of a dry, and preferably transparent, interlayer is proposed as an intermediary between the glass units. A preliminary research on different interlocking geometries and interlayer materials, presented in Chapter 7, pointed out that blocks following an osteomorphic geometry and interlayers made of polyurethane (PU or TPU) are the most promising for further development and validation of the system. Following the aforementioned findings, this chapter investigates by both experimental testing and numerical simulation the structural behaviour of an interlocking, dry-assembly made of osteomorphic cast glass blocks and PU as a dry interlayer.

8.2 Methodology

Initially different interlayers are cast in the desired form and are then placed between 2 half osteomorphic glass blocks to be tested under a static compressive load. Based on the experimental data, the most promising interlayer is selected for further investigating the influence of the interlocking geometry to the structural behaviour of the whole assembly. Accordingly, out-of-plane shear tests are performed in 3 series of assemblies, each made of 3 Type A blocks (as presented in the previous chapter) interleaved with the chosen interlayer. The blocks of each series have a different amplitude, namely 10, 15 and 20 mm. The set-ups and results of the experimental work are discussed in section 8.3. In respect to the findings of the experiments, a numerical FEM model of an osteomorphic assembly using a type B osteomorphic block is made to reconfirm the influence of the amplitude to the structural behaviour of the blocks, as well as to investigate the influence of the block's height to it. The aim of the numerical model is not to provide absolute design values, but to provide insights into the effects of all individual parameters in the overall performance. The numerical investigation is described in section 8.4. General conclusions and further recommendations are drawn in section 8.5 and 8.6 respectively.

8.3 Experimental

In brief, two different series of experiments using osteomorphic glass blocks and PU interlayers were carried out in order to investigate the mechanical behaviour of the proposed dry-assembled cast glass system:

- a compressive testing under static load of PU interlayers of different Shore Hardness and thickness.
- out-of-plane shear tests on assemblies of 3 glass blocks with different amplitudes

More specifically, initially, several series of compressive testing are carried out for PU interlayers of different Shore Hardness, between 60A – 80A and of different thickness, namely 3 and 6 mm. The interlayers, which are cast in the desired form, are placed between two half osteomorphic blocks, each measuring approx. 75 mm x 37.5 mm x 37.5 mm and tested under compression. The experiments and the relevant findings are discussed in sections 8.3.2 and 8.3.3 respectively. Based on the output of the first testing, the most promising interlayer is chosen to perform the out-of-plane shear tests on assemblies of various amplitudes, namely 10 mm, 15 mm and 20 mm. These are presented in section 8.3.4. All the prototypes have been produced in the Glass & Transparency Lab, by kiln-casting soda-lime osteomorphic glass blocks in two different scales and by manually casting two-component PU interlayers.

8.3.1 Materials

Glass blocks

The osteomorphic blocks, each measuring approximately 75 mm x 75 mm x 37.5 mm (full brick) or 75 mm x 37.5 mm x 37.5 mm (half brick), were kiln-cast at the *TU Delft Glass & Transparency Lab*. The moulds were made by the lost-wax technique. In specific, a 3D- printed full scale model of each interlocking design was used to create a silicone mould out of *Mould Max 30*. With this silicone mould, multiple wax models of the design were produced. *Crystalcast M248* investment material, in a powder to water volume ratio of 3:1, was poured around the wax models. Full brick moulds were made single, whereas half brick moulds were combined in pairs. The moulds were left to cure for an hour prior to steaming the wax out of the mould. *Schott B270*

modified soda-lime glass (main oxides as identified by the *XRF analysis* conducted at TU Delft: 71.8% SiO₂, 10.1% Na₂O, 6.3% K₂O, 5.2% CaO, 2.2% ZnO) was chosen for the production of the glass components. The amount of glass corresponding to each mould was introduced in the form of fragmented glass lenses (Ø75 mm) in terracotta flowerpots that were positioned above the moulds supported by 20 mm thick ceramic fiber strips (see Fig. 8.2). The glass blocks were kiln-cast at 970°C for 10 h and annealed between 540°C – 510°C, using a *ROHDE ELS 200 S Kiln* with 5-sided heating. The complete kiln-casting and annealing schedule can be seen in Fig. 8.1.

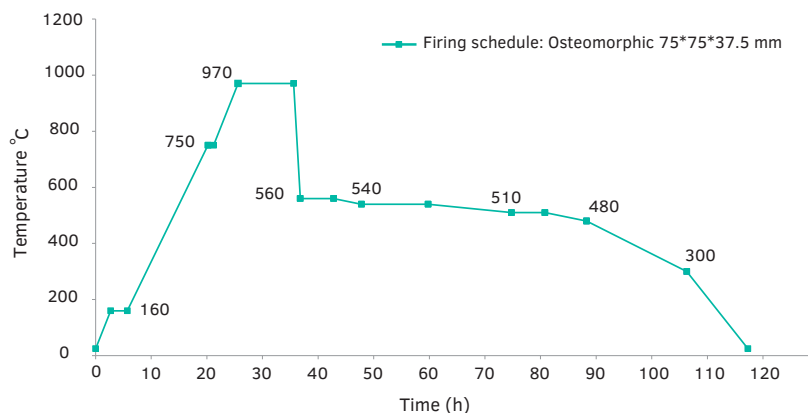


FIG. 8.1 Firing schedule followed for the kiln-casting and annealing of the osteomorphic blocks.



FIG. 8.2 From left to right: Arrangement of the glass-containing flowerpots above the crystal cast moulds and set-up of the kiln; View of the kiln at 970°C; Kiln-cast osteomorphic blocks prior to mould removal.

Afterwards, the face (top of the mould) from where the glass was poured was cut to size – to remove any excessive glass. The prototypes were then ground and polished

by a *Provetro* flat grinder machine. Specifically, the bottom face and the cut face of the blocks were ground and polished using diamond discs in a consecutive order of coarse to fine: 60, 120, 200 and 400 grit. A *Dremel* rotary tool with interchangeable diamond pads, similarly covering a range of 60 to 400 grit scale, was used to round the edges of the interlocking mechanism and eliminate possible imperfections at the interlocking wavy surface. There was no other post-processing on the other four faces of the blocks, including the interlocking surface. Due to the manual fabrication (and cutting of the one side), the bricks presented considerable size deviations (estimated to be $\pm 3\text{mm}$); the largest observed deviation was at the apex of the interlocking geometry.

Interlayer

Based on the criteria established in Chapter 7.6, readily available PU interlayers with a Shore Hardness between 60A - 80A were sought that could be cast in the desired shape. PU interlayers can be formed also by other techniques to the desired shape, such as vacuum forming or thermoforming, yet, two-component polymer casting was favoured as it guarantees an accurate, constant thickness throughout the interlayer's section. Table 8.1 gives an overview of the selected PU interlayer materials for the experimental validation of the system. Due to logistic reasons (availability of materials in the Netherlands as resins, etc.) most of the selected interlayers do not meet the transparency criteria. Even so, at this research stage the crucial factor to examine is to establish the most favourable Shore Hardness of the interlayer and thus, non-transparent interlayers were also considered when no alternative was readily available.

TABLE 8.1 Properties of a selection of cast PU interlayers available in the market as provided by the manufacturer

Material	Shore Hardness	Break El.	Tensile Strength	Die C tear strength	Colour
-	-	%	MPa	N/mm	-
PMC 746	60A	650	4.8	17.5	translucent amber
PMC 770	70A	750	5.2	35.1	translucent amber
Permacol 5450	75A/25D	unk	unk	unk	clear transparent
Task 16	80A/30D	233	15	34.5	light yellow

A two-part 3D-printed mould out of polylactic acid (PLA) was used for casting each PU resin to a constant 3 mm thick interlayer matching the osteomorphic geometry of the blocks (Fig. 8.3 and Fig. 8.4). Each specimen was manually poured into the mould and was left to cure for 24 h prior to removal. To prevent accidental direct contact of glass-to-glass at the edges, the cast interlayers are cast extending in all four sides.

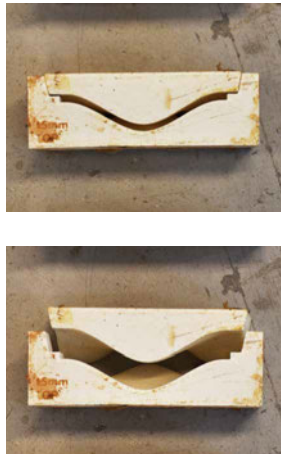


FIG. 8.3 Two-part 3D-printed mould out of PLA for casting the interlayers.



FIG. 8.4 Prototype of a 3 mm thick, cast PU interlayer.

8.3.2 Interlayer testing under compressive static load

8.3.2.1 Method

Fig. 8.5 shows the typical set-up of the experiment. Each interlayer was placed between two half osteomorphic glass blocks with 15 mm amplitude and tested in compression in a *Zwick Z100* universal testing machine at a rate of 250 N/s up to a given load, which was determined to be 40 kN⁶⁶. The use of cast glass blocks of the desired form was chosen to derive results that are representative of the system and shed light in the collaboration of the interlayer with complex surface geometries in glass. Each interlayer material was tested in a series of three specimens in order to derive statistical data. The specimens have been named according to their shore hardness and interlayer thickness as shown in Fig. 8.6.

⁶⁶ Due to human error, for some specimens a load of 40 kN was directly applied, without a gradually increasing load rate. Such specimens are represented by a linear slope until the set 40kN load at the F-u diagrams. Nonetheless, it is anticipated that this error does not alter the results of the creep performance of the interlayer under the given constant load.

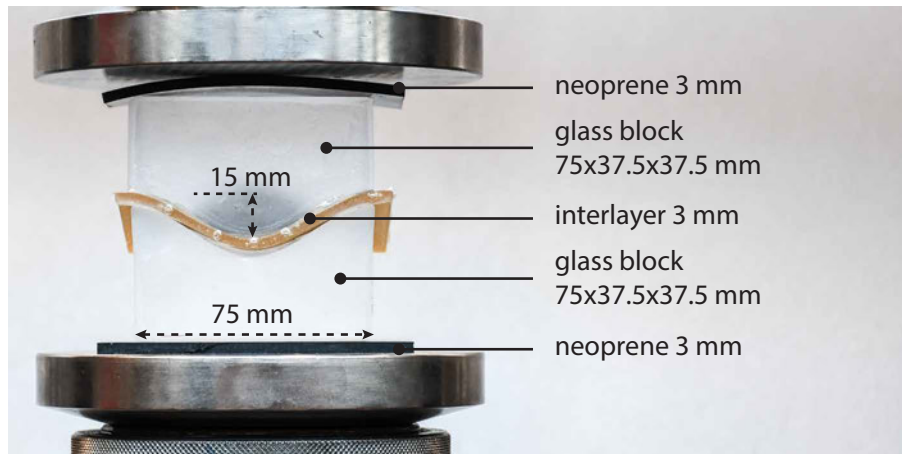


FIG. 8.5 Experimental set-up

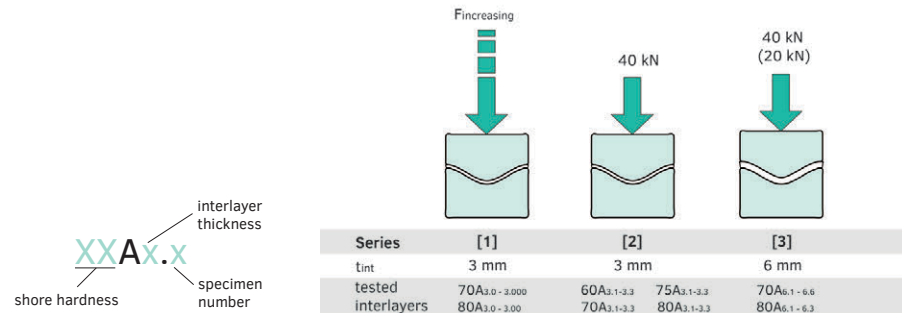


FIG. 8.6 Labelling principle of the specimens

FIG. 8.7 Schematic illustration and overview of the three series of experiments under compressive load on interlayers.

To prevent the failure of the system due to localized peak stresses occurring from the direct contact of glass with steel, 3 mm thick neoprene or 10 mm thick wood plates were placed between the steel plates of the machine and the glass assembly. The aim of this series of experiments is the evaluation of the interlayers' resistance under the given constant load; thus, the deformation under creep is regarded as the main output. Due to the influence of several external factors, such as the initial settling of the machine, the dimensional tolerances of the kiln-cast blocks, the initial deformation of the neoprene or wood intermediates and possibly the self-realigning (sliding) of the blocks in relation to each other upon initial loading, the early displacement of the assembly until the specimens reach the set static load is not considered as it is not representative of the interlayer's performance regarding creeping. To provide a comparison and evaluate the interlayer's contribution to the structural performance of the interlocking system, an assembly of two glass

blocks without interlayer in between is also tested in compression. In essence, three different series of compression tests are performed (Fig. 8.7):

Initially, a few specimens (namely $70A_{3,0} - 70A_{3,000}$ and $80A_{3,0} - 80A_{3,00}$) with 3 mm thick PU interlayers are tested in compression under higher loads in order to estimate the max. force that should be applied [Series 1]. Based on the results, it was determined to apply a max. load of 40kN to the next two series, corresponding to approx. 14.2MPa nominal compressive stress on the glass surface⁶⁷. Upon reaching the load of 40kN, the force is maintained constant for another 900s (15 min) in order to measure the deformation of the interlayer under creep. Accordingly, two series of specimens, first with PU interlayers of 3 mm thickness and then with PU interlayers of 6 mm thickness are tested [Series 2 and Series 3 respectively (see Fig. 8.8)].

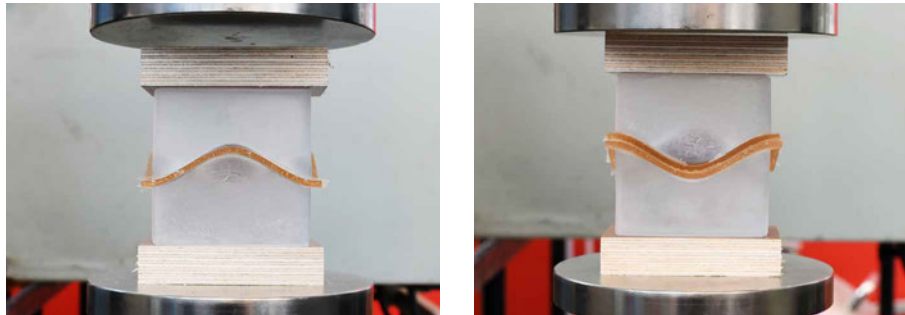


FIG. 8.8 Prototype with 70A interlayer of 3 mm thickness (left) and of 6 mm thickness (right).

8.3.2.2 Results

Table 8.2 summarizes the main results of the 3 series of experiments. The data have been processed so that only the deformation under creep (u_{creep}) is provided. Due to all the aforementioned reasons, the total displacement of the specimens in the (u-t) unprocessed graphs provided in this section is considerably higher than the 3 mm thickness of the interlayer. To compensate for the influence of the external factors all graphs are also presented showing only the deformation under creep mode. Thus, these graphs show the deformation over the last 900s of the tests. A minor effect by

⁶⁷ This compressive stress is already more than 70 times higher than the one imposed to the bottom array of glass blocks of the *Crystal Houses* façade due to the own weight of the construction (see chapter 5.6.5).

the deformation of the neoprene intermedium or/and of relevant sliding of the blocks is anticipated to still occur; however, these could not be isolated and quantified.

TABLE 8.2 Main results of the compression tests on PU interlayers.

Test Series	Specimen	t_{int}	F_{maxset}	$F_{fail.}$	T_{creep}	u_{creep}	intermediate	Failure mode
		mm	kN	kN	s	mm		
[1] Load Calibration	70A _{3.0}	3	-	72.5	-	-	neoprene	(a), (i)
	70A _{3.00}	3	-	57.8	-	-	neoprene	
	70A _{3.000}	3	-	63.5	-	-	neoprene	
	80A _{3.0}	3	60	60	66	0.6	neoprene	(a), (ii)
	80A _{3.00}	3	50	50	426	7.5	neoprene	
[2] 3mm thick interlayers	80A _{3.1}	3	40	-	900	0.9	neoprene	(c), (iv)
	80A _{3.2}	3	40	-	900	1.5	wood	
	75A _{3.1}	3	40	25.4 [†]	-	-	neoprene	(b), (i)
	75A _{3.2}	3	40	15.9 [†]	-	-	neoprene	
	75A _{3.3}	3	40	15.9 [†]	-	-	neoprene	
	70A _{3.1}	3	40	-	900	1.3	wood	(c), (iii)
	70A _{3.2}	3	40	-	900	1.1	wood	
	70A _{3.3}	3	40	-	900	1.8	wood	(c), (iv)
	60A _{3.1}	3	40	40	121	0.5	neoprene	(b), (ii)
	60A _{3.2}	3	40	40	58	0.8	neoprene	
	60A _{3.3}	3	40	-	900	0.7	neoprene	(c), (iii)
G _{glass}	0	40	4	-	-	neoprene	(i)	
[3] 6mm thick interlayers	70A _{6.1}	6-	20	-	900	0.9	neoprene	(c), (iii)
	70A _{6.2}	6-	20	-	900	1.0	neoprene	
	70A _{6.3}	6-	20	-	900	1.0	neoprene	
	70A _{6.4}	6-	40	-	900	1.0	neoprene	(c), (iii)
	70A _{6.5}	6-	40	-	2700	1.0	neoprene	(d), (iii)
	70A _{6.6}	6-	40	-	900	1.4	wood	(c),(iii)
	80A _{6.1}	6-	40	-	900	1.3	wood	(c), (iv)
	80A _{6.2}	6-	40	-	900	1.3	wood	
	80A _{6.3}	6-	40	-	900	1.5	wood	

(a) Failure of the glass blocks at their shortest section. No tearing of the interlayer observed.

(b) Perforation of the interlayer leading to glass to glass contact.

(c) assembly successfully withstood the max. set load for the scheduled 900 sec.

(d) assembly successfully withstood the max. set load for the scheduled 2700 sec.

(i) failure at increasing load

(ii) failure under creep mode

(iii) no failure – interlayer presented plastic deformation

(iv) no failure – interlayer presented no or negligible plastic deformation

[†] Test stopped when visible tearing of the interlayer was observed.

- applied as 2 x 3 mm

8.3.2.3 Series [1]: Load Calibration

Initially, different max. loads were set for the interlayers in order to determine the max. load for testing the specimens under creep. In specific, specimens interleaved with *PMC 770* (70A) and *Task 16* (80A) 3mm thick interlayers were tested on increasing load until failure. Specimens of the 70A series failed under an increasing load ranging between 56 – 72 kN. Accordingly, a max. load was set first to 60 kN and then to 50 kN. Although specimens of the 80A series successfully reached the max. set loads of 60 kN and 50 kN they failed shortly after due to creeping of the interlayer. In all cases failure occurred at the glass; no tearing of the interlayer was observed.

More specifically, all tested specimens failed with a consistent Y breaking pattern at the middle of their concave (shorter) section. The tip of the crack always originated at the apex of the concave section, as shown in Fig. 8.9. The peak stresses are assumed to have been caused by the insufficient (partial) contact of the interlayer at that area due to the increased manufacturing tolerances of the kiln-cast components. The shear stresses occurring in-plane at the interlayer due to its increasing deformation further contributed to failure (Fig. 8.10); this was especially evident in the case of the 80A specimens which failed under static load.

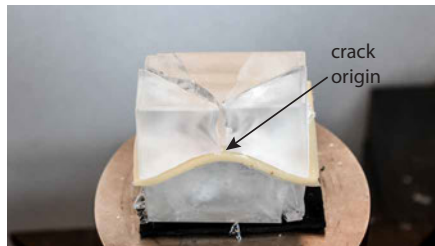


FIG. 8.9 Typical Y breaking pattern originating at the shortest section of the block (specimen 80A₁)

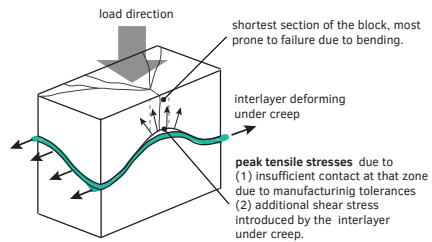


FIG. 8.10 Possible explanation of the cause of failure of the specimens interleaved with *PMC770* (70A) and *Task 16* (80A).

8.3.2.4 Series [2]: Compression testing of 3 mm thick interlayers

Based on the input from the first series of testing, it was determined to set the max. load to 40kN; upon reaching this force, it was set as a constant load and the specimen was maintained under it for 900s in order to evaluate the performance

of the interlayer under creep. Accordingly, 3mm thick interlayers of all 4 different selected PU materials (with a shore hardness ranging between 60A – 80A) were tested. The main results are summarized in Table 8.3.

TABLE 8.3 Main results of the compression tests on 3 mm thick PU interlayers (Series 2).

Specimen	t_{int}	F_{maxset}	$F_{fall.}$	T_{creep}	u_{creep}	intermediate	Failure mode
	mm	kN	kN	s	mm		
80A _{3,1}	3	40	-	900	0.9	neoprene	(c), (iv)
80A _{3,2}	3	40	-	900	1.5	wood	
75A _{3,1}	3	40	25.4 [†]	-	-	neoprene	(b), (i)
75A _{3,2}	3	40	15.9 [†]	-	-	neoprene	
75A _{3,3}	3	40	15.9 [†]	-	-	neoprene	
70A _{3,1}	3	40	-	900	1.3	wood	(c), (iii)
70A _{3,2}	3	40	-	900	1.1	wood	
70A _{3,3}	3	40	-	900	1.8	wood	(c), (iv)
60A _{3,1}	3	40	40	121	0.5	neoprene	(b), (ii)
60A _{3,2}	3	40	40	58	0.8	neoprene	
60A _{3,3}	3	40	-	900	0.7	neoprene	(c), (iii)
G _{glass}	0	40	4	-	-	neoprene	(i)

(b) Perforation of the interlayer leading to glass to glass contact.

(c) assembly successfully withstood the max. set load for the scheduled 900 sec.

(i) failure at increasing load

(ii) failure under creep mode

(iii) no failure – interlayer presented plastic deformation

(iv) no failure – interlayer presented no or negligible plastic deformation

[†] Test stopped when visible tearing of the interlayer was observed.

- applied as 2 x 3 mm

The results clearly demonstrate that interlayers with a comparably lower tear resistance, namely *Permacol 5450* (75A) and *PMC 746* (60A) are improper for the examined application. In particular, the assemblies interleaved with *Permacol 5450* (75A) and *PMC 746* (60A) failed due to the early tearing of the interlayer which lead to glass-to-glass contact. The testing of the 75A specimens (*Permacol 5450*) was aborted once visible perforation of the interlayer was noticed under considerably lower loads than the max. set 40 kN. The interlayer was always first torn at the sharpest edges of the interlocking blocks as can be seen in Fig. 8.11.

Specimens from the 60A series reached the max. set 40kN load; nevertheless, two of the three specimens (60A_{3,1} and 60A_{3,2}) failed soon after they entered the creep mode, due to the perforation of the interlayer, as shown in Fig. 8.12. Specimen

60A_{3.3} successfully withstood the constant 40kN force for 900s and reached an almost stable deformation under the given constant load. Nonetheless, upon the removal of the load, it was observed that the interlayer had presented evident plastic deformation: at the contact surface the interlayer had been plastically deformed to less than half of its initial thickness and had been locally perforated at the edges of the assembly, as shown in Fig. 8.13.

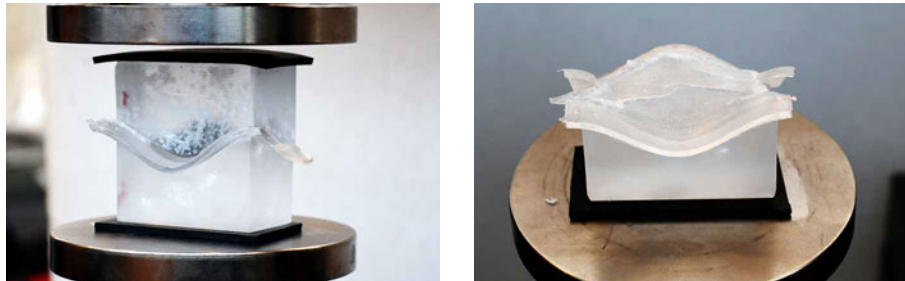


FIG. 8.11 75A specimen after the test was aborted due to visible tearing of the interlayer.



FIG. 8.12 Typical glass failure originating at the edge of the assembly caused by the perforation/tearing of the interlayer (specimen 60A₁)

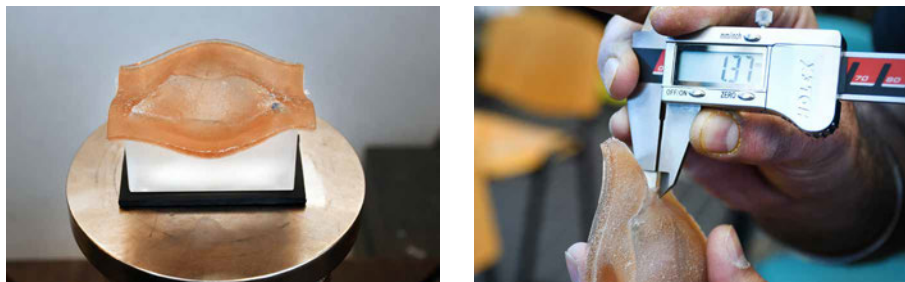


FIG. 8.13 Specimen 60A₃ after the completion of the test. There is evident plastic deformation.

In comparison, specimens interleaved with 70A and 80A interlayers successfully withstood the 40 kN load for 900s. Specimens $80A_{3,1}$, $80A_{3,2}$ and $70A_{3,3}$ did not present any visible plastic deformation after the testing (see Fig. 8.14). Specimens $70A_{3,1}$ and $70A_{3,2}$ presented limited plastic deformation at the contact area of the interlayer with the glass blocks.



FIG. 8.14 One of the 80A interlayer specimens during (right) and after (left) testing. No visible plastic deformation was observed.

Nonetheless, the deformation of both 70A and 80A interlayer materials remained time-dependant for the duration of the creep testing, as indicated by the deformation in time curve $[u - t]$ of the specimens, shown in Fig. 8.15. Without reaching a stable deformation (which would be expressed as a horizontal line in the $[u-t]$ diagram) it is difficult to predict if the tested interlayers would successfully sustain the given load for a longer period.

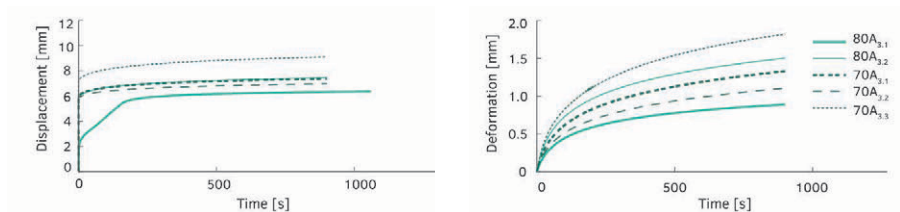


FIG. 8.15 Displacement in time graph of $70A_{3,x}$ and $80A_{3,x}$ specimens (left) and processed so that only the deformation in time under the static 40 kN load is shown (right)

Finally, in comparison to the specimens with interlayer in-between, the G_{glass} specimen, in which there was direct glass to glass contact, failed at a considerably lower load of just 4kN, at the sharpest edge of the assembly (Fig. 8.16), similar to the specimens that failed due to tearing of the interlayer. The failure load of the

G_{glass} specimen -which is 10 times less than the 40kN load that the 70A and 80A specimens could resist- highlights the importance of a soft-interlayer for enhancing the structural performance of the assembly. It should be noted that the failure load of this specimen corresponds to a nominal compressive stress of approx. 1.4 MPa – a value considerably less than the failure stress value of the rectangular solid glass blocks tested without an interlayer in Chapter 5.6.1. This difference in strength can be partially attributed to the kiln-cast fabrication and manual post-processing of the osteomorphic blocks compared to the hot-poured and CNC polished solid glass blocks of the *Crystal Houses* façade. The interlocking geometry has a significant influence on the resistance of the blocks against localized stresses as well: compared to the flat geometry of the *Crystal Houses* blocks, the complicated geometry of the contact surface of the blocks is more prone to the generation of peak tensile stresses.



FIG. 8.16 Failure mode of glass specimen without the use of an interlayer.

Overall, it was concluded from these experimental series that the examined 60A and 75A interlayer materials are not appropriate for the selected structural application due to their low tear strength. Both 70A and 80A interlayer materials are considered promising candidates. From the 1st series it was observed that due to the manual casting and post-processing of the glass blocks, dimensional deviations higher than 3 mm occur at the interlocking surface – particularly at the apex of the interlocking mechanism – which cannot be fully compensated by a 3 mm thick interlayer. This in turn, leads to stress concentrations at the points where there is insufficient contact

between glass and interlayer, which leads eventually to failure, even during static load due to the shear stresses caused by the creeping of the interlayer. This was manifested by the failure mode of the specimens tested in Series [1] and has as well been indicated by the experimental work of (Aurik et al. 2018). Hence, to further validate the mechanical behaviour of the assembly, a third series of experiments was carried out, similar to the last one but employing interlayers of 6 mm thickness.

8.3.2.5 Series [3]: Compression testing of 6 mm thick interlayers

After evaluating the previous two series of testing, it was determined to further test interlayer variants of 6 mm thickness under a constant 40kN load for 900s in order to evaluate if thicker interlayers perform better under creep mode⁶⁸. This series of experiments was carried out only on 70A and 80A interlayer specimens, which demonstrated satisfactory tear and creep resistance in the previous series of experiments. Due to time restrictions it was determined to apply the 6 mm interlayer as two layers of 3 mm⁶⁹. The two 3mm thick interlayers were simply placed on top of each other and positioned in between the two glass blocks (Fig. 8.21 and Fig. 8.22). A series of 70A specimens was also tested under creep with a set constant load of 20 kN, which results to a nominal compressive stress (approx. 7 MPa) that is closer to the one anticipated in a real application. In all the specimens 3mm neoprene or 10mm thick hard wood plates were used as intermediary between the steel head of the machine and the glass blocks.

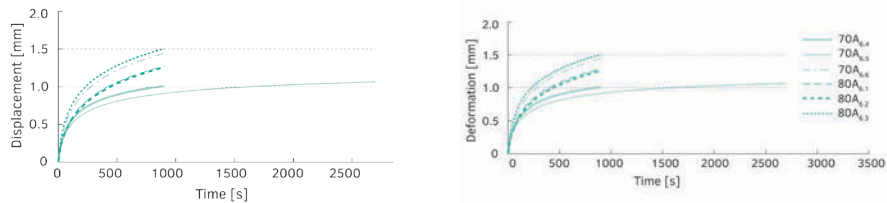


FIG. 8.17 Displacement in time ($u - t$) graph for the 70A and 80A 6 mm thick specimens tested to 40kN load for 900 s (left) and processed so that the deformation in time is shown only during the static 40 kN load (right).

⁶⁸ In some of the specimens the 40kN load was accidentally imposed instantly, without a constant increasing rate of 250 kN/s. This results in a completely straight initial line at the [F-u] diagrams (as there was a 0 N force and then instantly a 40 kN force) and to a vertical initial line at the [u - t] graph.

⁶⁹ Due to time restraints that did not allow for the manufacturing of a second 3D-printed mould for the casting of the interlayers, it was determined to use 2 times 3 mm thick interlayers to estimate the performance of a 6mm thick variant.

The corresponding deformation in time [u-t] graph, both unprocessed and processed so that the initial displacement due to external factors is compensated, can be seen in Fig. 8.17. The main results are summarized in Table 8.4.

TABLE 8.4 Main results of the compression tests on 6 mm thick PU interlayers (Series 3).

Specimen	t_{int}	F_{maxset}	F_{fall}	T_{creep}	u_{creep}	intermediate	Failure mode
	mm	kN	kN	s	mm		
70A _{6.1}	6	20	-	900	0.9	neoprene	(c), (iii)
70A _{6.2}	6	20	-	900	1.0	neoprene	
70A _{6.3}	6	20	-	900	1.0	neoprene	
70A _{6.4}	6	40	-	900	1.0	neoprene	(c), (iii)
70A _{6.5}	6	40	-	2700	1.0	neoprene	(d), (iii)
70A _{6.6}	6	40	-	900	1.4	wood	(c),(iii)
80A _{6.1}	6	40	-	900	1.3	wood	(c), (iv)
80A _{6.2}	6	40	-	900	1.3	wood	
80A _{6.3}	6	40	-	900	1.5	wood	

(c) assembly successfully withstood the max. set load for the scheduled 900 sec.

(d) assembly successfully withstood the max. set load for the scheduled 2700 sec.

(iii) no failure – interlayer presented plastic deformation

(iv) no failure – interlayer presented no or negligible plastic deformation

- applied as 2 x 3 mm

All specimens successfully withstood the set 40 kN (or 20 kN) load for 900s. In particular, none of the 80A specimens had “plastic” deformation after the removal of the load. In comparison, the 70A specimens clearly had visible plastic deformation at the contact area of the interlayer with the glass blocks (see Fig. 8.23).

Overall, the 70A specimens showed less deformation (1.0 – 1.4 mm) during the creep mode than the 80A variants (1.3 – 1.5). The 80A specimens showed similar creep resistance in both 3 and 6 mm thickness and a rather broad range of deformation under creep in both cases as can be seen in Fig. 8.18.

The 6 mm thick 70A interlayers had a relatively stiffer and more consistent behaviour under creep compared to the 3 mm variant: all 3 specimens (70A_{6.4} – 70A_{6.6}) showed between 1.0-1.4 mm total deformation under creep compared to 1.1-1.8 mm of the 70A_{3.1} – 70A_{3.3} specimens (see Table 8.2 and Fig. 8.19). In particular, specimen 70A_{6.5}, which was subject to a 40kN constant load for 2700s, showed the closest approximation to a horizontal slope at the (u-t) diagram shown in Fig. 8.19; in the last 1450 s of the test the interlayer deformed by 0.1 mm. It is unclear if this deformation can be attributed to the interlayer material or the neoprene used as intermediate between the glass blocks and the steel machine, or both. The 70A

specimens tested in compression under a constant load of 20kN ($70A_{6.1} - 70A_{6.3}$) presented a nearly consistent deformation under the creep test duration, equal to 0.9 – 1.0 mm (Fig. 8.20), comparable to the deformation of similar specimens tested under double the load.

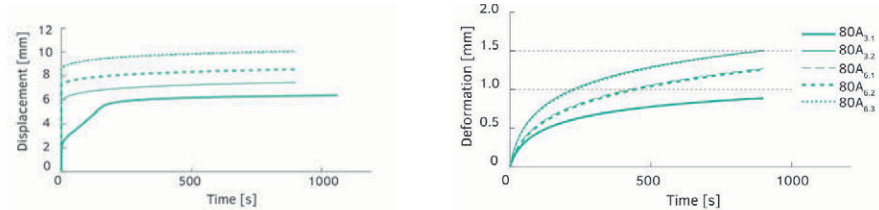


FIG. 8.18 Displacement in time ($u - t$) graph for the 80A interlayer specimens of 3 mm and 6 mm thickness tested under 40 kN load for 900s (left) and processed graph so that the deformation in time is shown only during the set 40kN constant load (right).

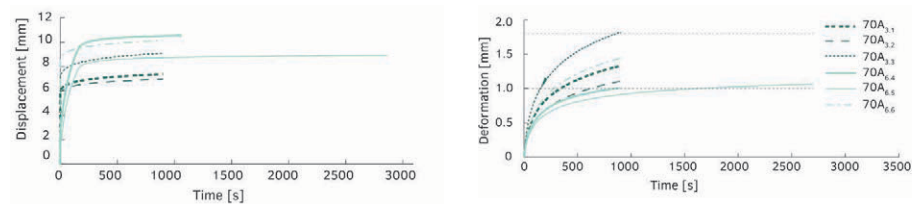


FIG. 8.19 Displacement in time ($u - t$) graph of 70A interlayer specimens of 3 mm and 6 mm thickness tested under a static 40 kN load for 900 s (left) and processed graph so that the deformation in time is shown only during the static 40 kN load (right).

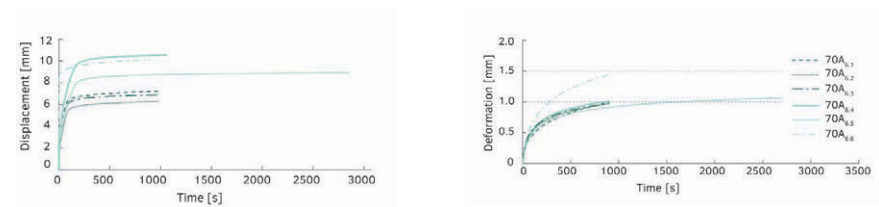


FIG. 8.20 Displacement in time ($u-t$) graph for 70A interlayer specimens, 6 mm thick tested under 20 kN ($70A_{6.1} - 70A_{6.3}$) and 40 kN ($70A_{6.4} - 70A_{6.6}$) load for 900s (left) and processed graph so that the deformation in time is shown only during the set constant loads (right).

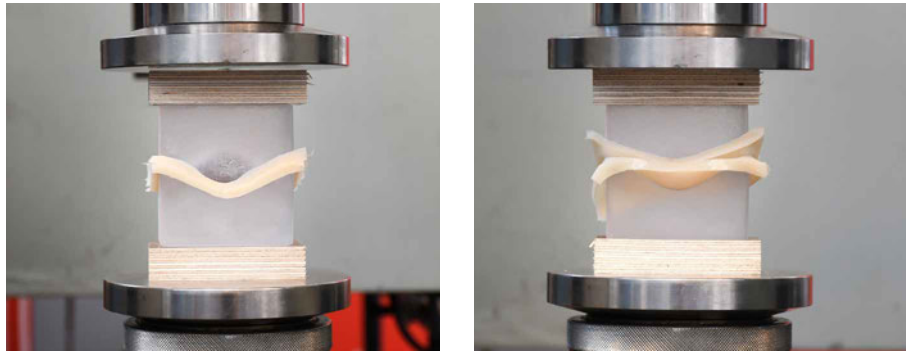


FIG. 8.21 A 6 mm thick 70A specimen before (left) and during (right) resting under 40 kN constant load

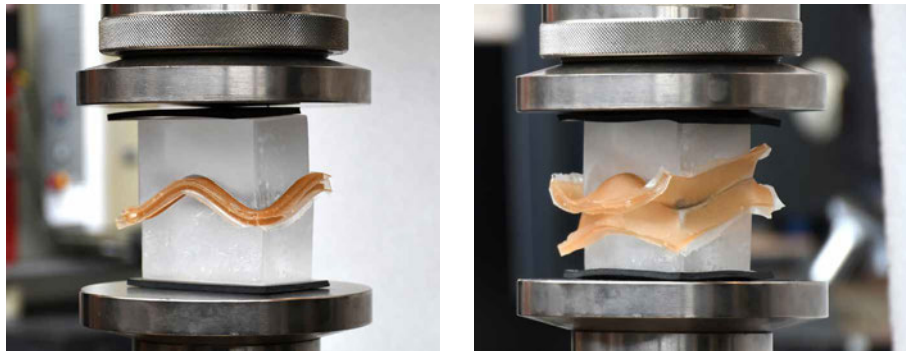


FIG. 8.22 A 6 mm thick 70A specimen, before (left) and during (right) testing under 40 kN constant load.



FIG. 8.23 Visible plastic deformation of 70A specimen directly after the completion of the test.

8.3.3 Conclusions on Interlayer material

Three different series of specimens out of kiln-cast glass interlocking blocks interleaved with different cast PU interlayers were tested under compression as follows:

- 1 3 mm thick interlayers were tested until failure by a constantly increasing compressive load
- 2 3 mm thick interlayers were tested in compression up to a max. set load of 40 kN; upon reaching that value the load was maintained constant for 900 s.
- 3 6 mm thick interlayers were tested in compression up to a max. set load of 40 kN; upon reaching that value the load maintained constant for 900 s.

Table 8.5 summarizes the main findings of each series. Overall, it can be derived that the creep and tear resistance of the interlayer are of crucial importance to the structural performance of the interlocking assembly.

TABLE 8.5 Summary of the main results of the interlayer testing.

Series	Interlayer applied	t_{int} mm	No of Specimens	$F_{max.set}$ kN	Creep mode s	Failure mode/ observations
1	70A	3	3	-	-	(a ₁)
	80A		2			
2	60A	3	3	40	900	(a ₂)
	70A		3			(b ₁)
	75A		3			(a ₂)
	80A		2			(b ₂)
3	70A	6	6	20 / 40	900 (2700)	(b ₁)
	80A		3	40	900	(b ₂)

(a₁) Failure due to insufficient contact of the interlayer at the concave-convex interlocking area of the blocks, combined with the shear stresses occurring at the interlocking surface due to the increasing deformation of the interlayer under constant or increasing load.

(a₂) Failure due to penetration of the interlayer leading to glass-to glass contact

(b₁) No failure – visible plastic deformation

(b₂) No failure – no observable plastic deformation

In the first series [1] all specimens failed under increasing or constant (≥ 50 kN) load due to insufficient contact of the interlayer at the concave-convex interlocking area of the blocks, combined with the shear stresses occurring at the interlocking surface due to the increasing deformation of the interlayer. Although in several of the specimens the assembly reached the maximum set load without cracking, the

continuous deformation of the interlayer under static load thereafter introduced further tensile stresses that eventually lead to failure of the glass elements. Accordingly, it was determined to set the max. load to 40 kN for the next 2 series. In addition, the aforementioned failure mode of the specimens indicated that due to the manual fabrication and post-processing of the kiln-cast blocks an interlayer thicker than 3 mm might be essential for preventing the generation of localized peak stresses due to the insufficient surface contact between the glass and the interlayer.

In the second series [2] of experiments, it was derived that interlayers with a lower tear resistance, namely *Permacol 5450 (75A)* and *PMC 746 (60A)* are unsuitable for the examined structural application due to the penetration of the interlayer, which leads to the eventual glass-to-glass contact and thus to failure at lower stress values. On the contrary, all 70A (*PMC 770*) and 80A (*Task 16*) specimens were able to successfully withstand the set 40kN constant load for 900s. Nonetheless, none of the interlayer specimens stabilized within the 900 s interval at the given load and interlayer thickness: in all cases, the deformation in time (u-t) graph of the specimen indicated that the interlayers were creeping through the duration of the test. If the test had been programmed for a longer duration, failure would have possibly occurred similar to the one described for the first series due to the increased dimensional tolerances of the blocks in combination with the increasing shear stresses imposed within the interlayer due to creep. Thus, it was determined to further validate these two more promising materials in a larger thickness, of 6 mm, under the same constant load of 40 kN for 900s. It was also determined to test one of the series to a constant 20 kN load, which corresponds to a nominal compressive stress that is in closer proximity to the one anticipated in an actual construction.

Indeed, the results of the third series [3] showed that the thicker variants behave stiffer under compression. This is particularly the case for the 70A_{6,x} specimens, which deformed less in creep than the 3 mm variants (70A_{3,x}). The 70A_{6,5} specimen, which was the only one tested under creep for 2700s, presented an almost stable deformation after approx. 1300s. This suggests that the examined interlayer could possibly reach equilibrium if tested for longer duration and present the desired time-independent deformation. This, however, is yet to be experimentally confirmed.

Although the 70A specimens presented apparent plastic deformation, whereas the 80A did not, the former presented a comparatively more horizontal slope in the deformation in time (u-t) curve and better creep resistance than the latter. Thus, *PMC 770 (70A)* of 6 mm thickness was determined to be used in the out-of-plane shear experiments, described in the following section. It is considered that the 80A interlayer is an equally promising candidate for further investigation.

From the interlayer testing several more important outcomes were withdrawn regarding the geometry of the interlocking glass units:

The experiments demonstrated that an insufficient fillet radius at the edges of the interlocking mechanism can lead to local perforation of interlayers with lower tear resistance and in turn to the early failure of the assembly due to glass-to-glass contact. Thus, smoother changes in curvature along the interlocking surfaces are preferred.

Another conclusion regarding the interlocking geometry derived from the tests is that the greater the amplitude of the interlocking system, the more sensitive the assembly is to manufacturing intolerances and thus to the introduction of peak tensile stresses because of insufficient contact (mismatch) and collaboration between the interlayer and the glass units. This can be improved either by introducing a thicker interlayer (4-6 mm), which however would further compromise the stiffness of the assembly, or by a smoother interlocking mechanism.

8.3.4 **Shear tests on osteomorphic blocks with different amplitude height**

8.3.4.1 **Method**

Aim of this experiment is a comparative evaluation of the mechanical performance of blocks of various amplitudes and to investigate the effect of the geometry of the interlocking mechanism to the structural behaviour of the assembly. The block's amplitude height is defined as the distance between the planes of the highest and lowest points of the interlocking mechanism. Accordingly, assemblies out of osteomorphic blocks with different amplitudes, namely 10 mm, 15 mm and 20 mm, were tested in out-of-plane shear, in series of 3 specimens each (see Fig. 8.24). An illustration and a photograph of the experimental set-up can be found in Fig. 8.25 and Fig. 8.26 respectively.

Based on the output of the experimental testing on the interlayer material it was determined to apply 6 mm thick 70A interlayers in between the blocks of each assembly to ensure the full contact of the interlayer and the blocks and the even spread of stresses. Accordingly, each assembly consists of 3 blocks - two halves and one full block in the middle - which are interleaved with 6 mm thick 70A interlayers

in between. A steel frame stabilizes and supports the assembly. The frame is pre-compressed by two steel threaded rods in a plane vertical to the applied load. The pre-compression of the rods is applied by a mechanical torque wrench set in a consistent, low pre-stress, value. The set-up is flipped by 90 degrees when the pre-compression is applied in order to facilitate the self-alignment of the blocks; after pre-compressing the assembly, it is flipped back to a horizontal position. Soft 3 mm thick neoprene interlayers are placed as intermediary between the glass blocks and the steel plates. A soft aluminium rectangular bar, 20 mm wide is placed under the steel bar that applies the deformation force to the assembly. The aluminium bar allows the accurate measurement of the deformation of the middle glass block, without introducing concentrated stresses to the glass surface. All the tests are carried out in a Zwick Z100 displacement-controlled universal testing machine at a loading rate of 5 mm/min.

It should be noted that due to the manual fabrication of the blocks, some of the specimens would self-align in a shifted position compared to each other. Due to the resulting eccentricity, the load was not applied in an absolutely vertical direction.

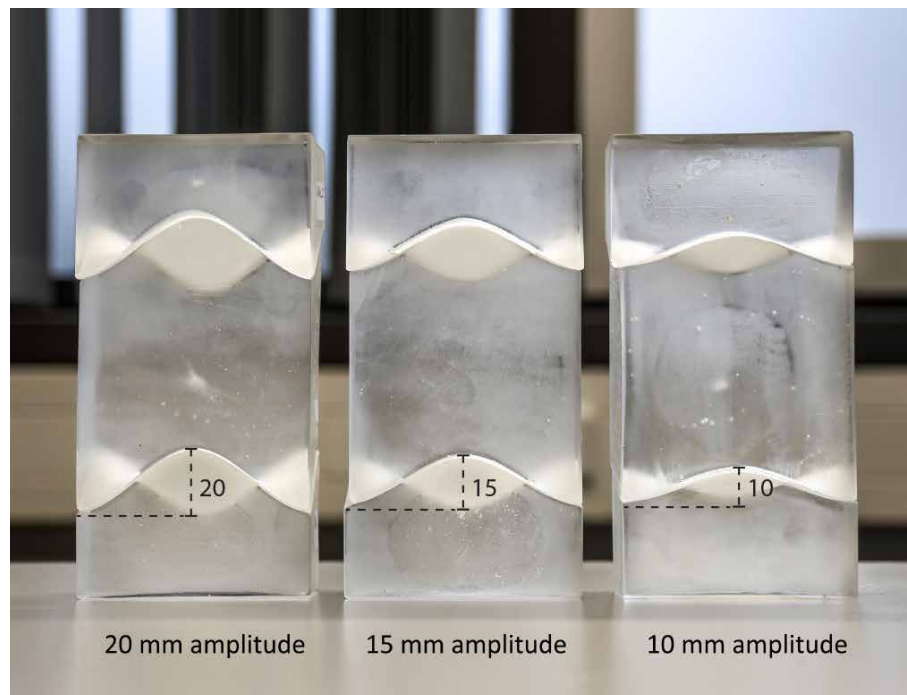


FIG. 8.24 Assemblies (without the use of an interlayer) of blocks with the different examined amplitudes.

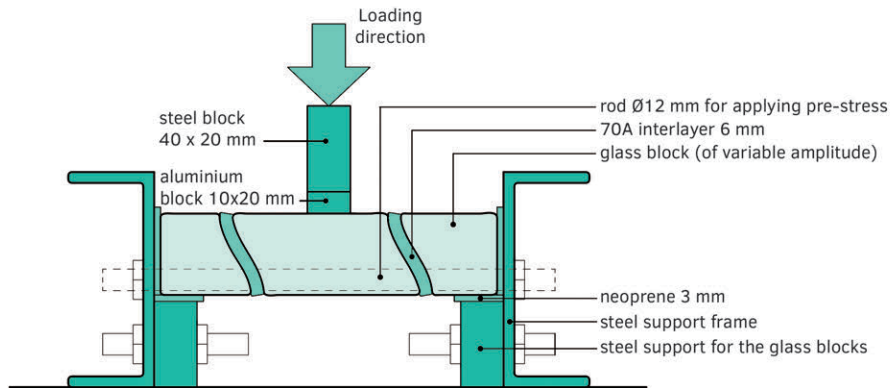


FIG. 8.25 Illustration of the experimental set-up.

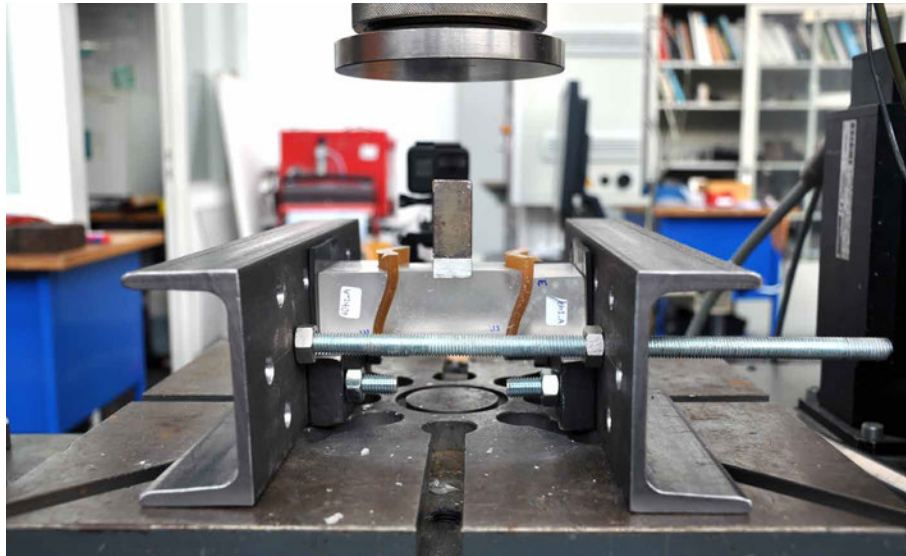


FIG. 8.26 Experimental set-up

8.3.4.2 Results

Table 8.6 summarizes the main results. The Standard Force vs displacement (F-u) graph of all specimens can be seen in Fig. 8.27. The tests were stopped when there was evident cracking of the blocks which resulted in a significant loss of load-carrying capacity.

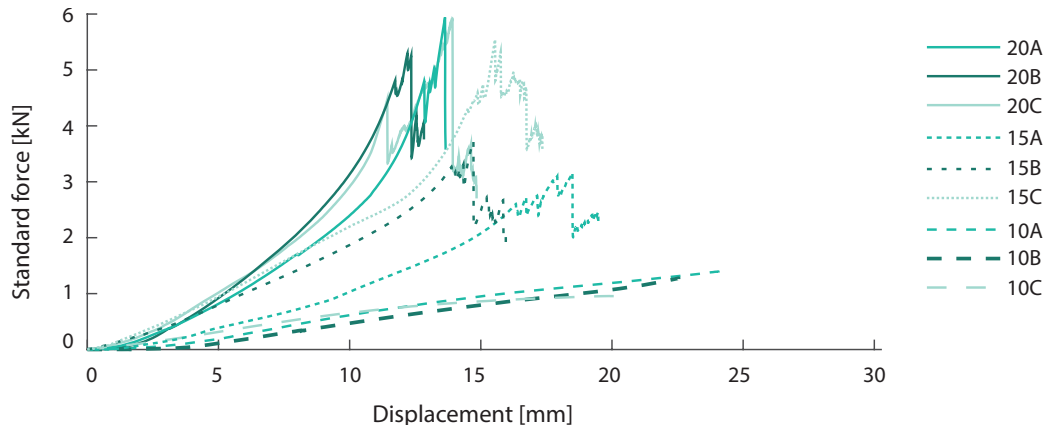


FIG. 8.27 Displacement - Standard Force diagram for all specimens

TABLE 8.6 Summary of the main results

Series	Specimen	F_{crack} [N]	U_{crack} [mm]	Cracked blocks H: side block M: middle block	Remarks
10	A	1410	24.1	-	(i), (ii)
	B	1280	22.5	-	(i), (ii)
	C	967	20.5	-	(i), (ii), *
15	A	3170	19.5	M	(ii), (a), *
	B	3740	15.9	M	(ii), (a)
	C	5553	17.3	H, M	(ii), (a), *
20	A	5950	13.6	H, M	(ii), (a), (b), *
	B	5310	12.8	M	(ii), (a)
	C	5930	14.8	H, M	(ii), (a), (b), *

(i) test aborted when the total deformation (incl. initial deformation of the settling of the machine) was 25 mm. No damage occurring at the blocks, nor plastic deformation of the interlayer.

(ii) visible shifting of the middle block downwards with increasing load

(a) crack initiated close to the change of interlocking curvature of the middle block

(b) crack initiated close to the change of interlocking curvature of the half block

* load was applied in a slightly inclined direction due to the initial misalignment of the assembly

The following main conclusions were drawn from these experimental series:

- All specimens showed visible deflection, expressed as the shifting of the middle block downwards, prior to failure. This is because the blocks are in principle free to rotate. The resistance to the bending moment is provided by the peripheral constraint force, which in the experimental set-up is considerably low. This in turn results to a limited load-bearing capacity of the system prior to failure. Yet, the low bending stiffness

of the assembly can also be seen as a warning mechanism that allows for increased safety in a structure, due to its pseudo-ductile behaviour prior to failure.

- As expected, the specimens had localized failure and thus, an effectively increased damage tolerance compared to a monolithic variant: cracks do not spread from one element to another in the specimens. In the cases where two blocks would crack, this would happen non-simultaneously and occurs at different locations (see Fig. 8.31 and Fig. 8.32).
- Blocks with a higher interlocking amplitude are in principle more favourable as they present a higher shear capacity and stiffness and fail at less deformation (see Fig. 8.28).
- Internal flaws (within the meso-structure of the blocks) or defects at locations that are not anticipated to be subject to peak stresses do not seem to compromise the overall performance of the assembly. Actually all specimens failed at the same locations; either at the edges or close to the middle of the interlocking mechanism.
- After removal of the load, all specimens tended to resettle towards their original configuration; yet the assemblies remained visibly misaligned (Fig. 8.29, Fig. 8.30, Fig. 8.31).
- Higher pre-stress values and the use of thinner interlayers are essential for obtaining a stiffer assembly/system.
- The relatively low dimensional accuracy of the kiln-cast components has influenced the structural performance of the specimens. Yet, due to the magnified effect of such deviations, they also revealed that the examined geometry is prone to eccentricity during assembly caused by the sliding of the components relevant to each other. The resulting eccentricity is higher as the amplitude increases.

In general, the specimens of each series presented relatively consistent failure values and stiffness curves, as can be seen in Table 8.6 and in the F-u diagram of Fig. 8.27. Overall, it can be inferred that the higher the amplitude, the stiffer the behaviour of the assembly is, failing at higher loads and at less deformation. More specifically, specimens with 20mm amplitude failed at approx. 5 times the load and at almost half the deformation compared to specimens with half the amplitude (10mm) (see Fig. 8.28). From the graph of Fig. 8.27 it can also be observed that the stiffness of the specimens with 15mm amplitude is closer to the one of the 20mm variant than the 10mm one.

In all three series, the middle block was evidently shifted downwards, prior to cracking (see Fig. 8.28). This high deformation is attributed primarily to the low pre-stress value applied (the threaded rods were loosely fastened) and secondly to the relatively thick interlayer of 6mm, essential for accommodating the dimensional discrepancies of the manually fabricated glass blocks. The dimensional deviations, combined with the necessity for a relatively thick interlayer, have also resulted in many cases into an initial eccentricity of the assembly during installation in the test rig. The relatively low forces at failure can also be attributed to the low bending stiffness of the specimens.

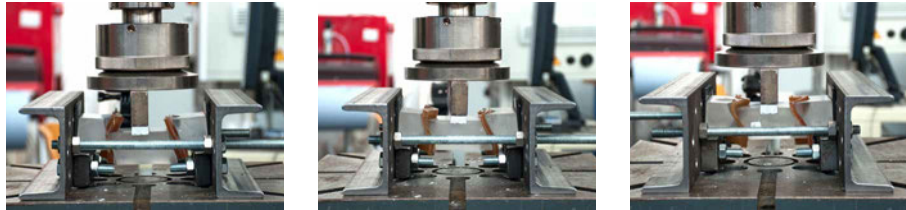


FIG. 8.28 Maximum deformation prior to failure of assemblies with blocks of 10 mm (left), 15 mm (center) and 20 mm (right) amplitude. The tests with blocks of 10 mm amplitude were aborted once the assembly reached an apparent deformation of 25 mm.



FIG. 8.29 Assembly of block with 10 mm amplitude before (left), during (centre) and after testing (right). It can be seen that upon load removal the assembly is self-realigned towards its original configuration.

More specifically, the testing of the 10mm amplitude series was aborted when the total deformation (including the initial settling of the testing machine) reached 25mm. There were no cracks observed at any of the specimens, yet the middle block in all cases had slid almost entirely out of the assembly (Fig. 8.29). In this case, the insufficient pre-compression applied at the external frame and the accumulated thickness of all the interlayers (two 6 mm PU sheets and two 3 mm neoprene sheets) could allow the slide-out of the middle block of just 10 mm amplitude. When the load was removed the assembly self-realigned towards its initial configuration. Due to time restrictions the assembly had to be removed a few minutes after testing and

thus it was not checked if the specimen would eventually resettle fully to its original position. The other two assemblies behaved similarly, with the 20mm amplitude series presenting the highest shear capacity.

In all specimens of the series of 15mm and 20mm amplitude, failure occurred at the interlocking surface, in particular, either close to the middle of the side interlock, where there is a change in interlocking curvature⁷⁰ (see Fig. 8.30, Fig. 8.31 and Fig. 8.32) or at the edges of the blocks. In specific, after the middle block has shifted downwards, the assembly becomes stiffer. This appears at the F-u diagram in Fig. 8.27 as a change to a steeper inclination of the specimens prior to failure. The stiffening can be attributed to an increased contact area after the resettling of the individual components. Upon stiffening, high peak stresses are generated at the upper part of the middle block. As a result, all specimens consistently failed at the middle block. Owing to the fragmented nature of the system, there was no crack propagation to the adjacent blocks. When one of the support (half) blocks also failed, the crack in the latter would again initiate from one of the locations where the curvature changes at the interlocking surface. This could be either in close proximity to the point of origin of the initial crack of the middle block or to a completely different location (e.g. on the other interlocking side of the block) (see Fig. 8.32). There was no plastic deformation observed at any of the interlayers. In some cases, due to the energy released by the crack, the interlayer would be locally sliced from the glass fragments after failure had occurred.

An important observation derived from the experimental set-up itself, is that the examined interlocking geometry is prone to eccentricity during assembly due to the limited number of interlocking shear keys. The higher the amplitude the more the resulting eccentricity due to manufacturing dimensional tolerances, as blocks tend to slide away from each other. Thus, although the highest amplitudes are preferable for shear resistance and reduced global deformations, they are also the most prone to induce eccentricity to the assembly. An interlocking mechanism of average amplitude, i.e. in this case 15 mm, is in this case considered the best compromise between shear capacity and accuracy in construction. In addition, the design of an interlocking mechanism with multiple locks, such as the Type B osteomorphic block presented in sections 7.5.2 and 7.5.3 is suggested as a more favourable form: the multiple interlocking locks of this geometry enhance the self-aligning capacity of the components, and to this extent, of the resulting structure as well.

⁷⁰ This location is different to the one anticipated by the numerical model described in chapter 8.3 as the latter has been made to simulate in-plane shear stresses.

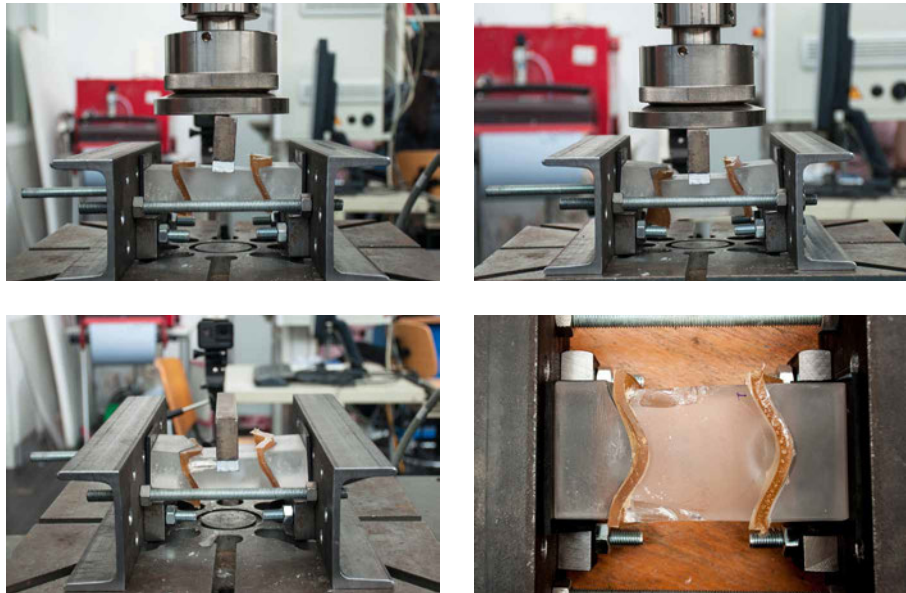


FIG. 8.30 Specimen out of blocks with 15 mm amplitude before testing (top left); at max. deformation (top right); and after failure (bottom left and right).

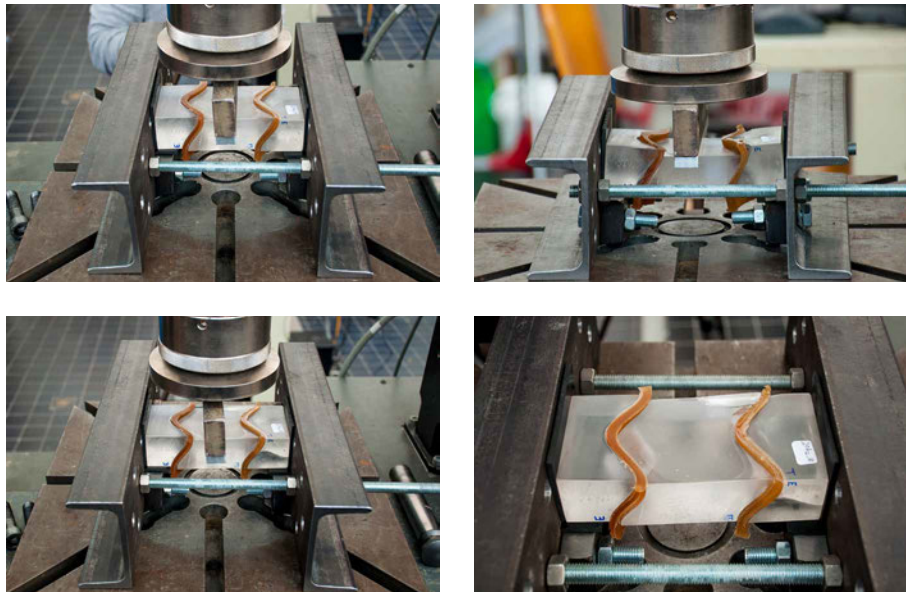


FIG. 8.31 Specimen out of blocks with 20 mm amplitude before testing (top left); at max. deformation (top right); and after failure (bottom left and right)

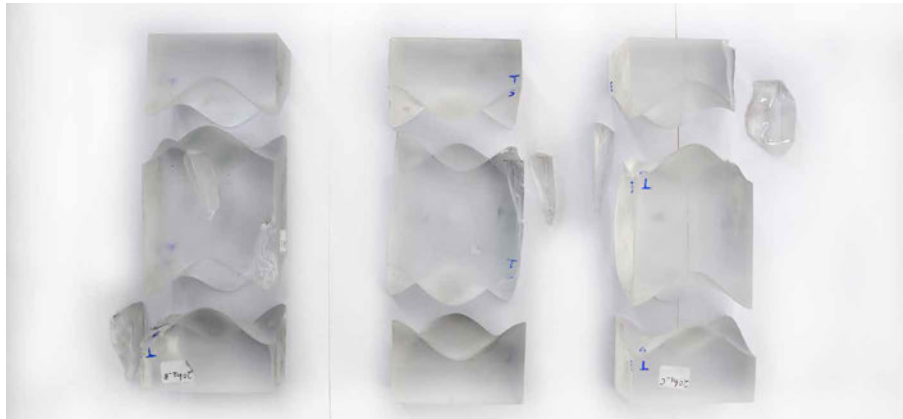


FIG. 8.32 Specimens out of blocks with 20 mm amplitude after testing. It is evident that the crack in adjacent blocks are not continuous.

8.4 Numerical investigation of the interlocking geometry of the osteomorphic blocks

8.4.1 Model set-up

The experiments indicated that higher amplitudes are more favourable in terms of shear capacity, yet they are as well more prone to eccentricity caused by dimensional deviations. A solution to this is the design of an interlocking unit with multiple shear keys, which enhance its self-alignment capacity, such as Type B block described in section 7.5.2. Moreover, the experiments suggested that for the manufactured kiln-cast specimens a thicker than 3 mm interlayer is necessary to accommodate the dimensional discrepancies. The thicker the interlayer, the more compromised becomes the stiffness of the entire assembly. In case that industrially manufactured glass blocks are used, it is anticipated that interlayers between 3-4mm thickness should suffice for accommodating the dimensional discrepancies of the individual blocks but also of the entire construction.

Accordingly for the numerical model, developed by (Jacobs 2017), an osteomorphic block with multiple locks, similar to Type B⁷¹ form (discussed in Chapter 7, see Fig. 7.10) is used. The reference brick dimensions are 300x150x150 mm. The geometry of this block is generated by multiplying type A block –used in the previous experiments– four times and scaling it up by a factor of 2 (see Fig. 8.33). A 4 mm 70A PU interlayer is simulated as the intermediate between the blocks.

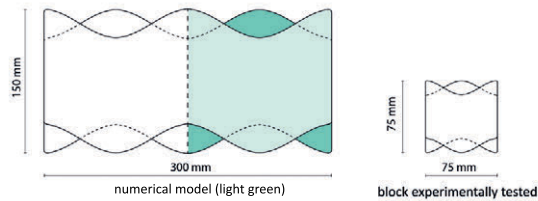


FIG. 8.33 Numerical model (Type B block) vs experimentally tested block (Type A).

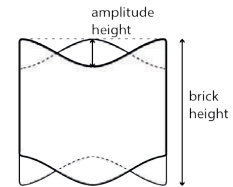


FIG. 8.34 Definition of block height and amplitude height.

Aim of the model is to further assess the influence of the most crucial geometrical aspects of the interlocking mechanism, namely the amplitude and the brick height, to its structural performance.

The amplitude height of each block is defined as the distance between the planes of the highest and lowest points of the interlocking mechanism, as shown in Fig. 8.34. The studied range concerning the block height is from 40mm to 150mm and the amplitude height is from 5mm to 20mm. A detailed description of the model set-up can be found in (Jacobs 2017). The geometry of the block is generated through the Grasshopper plug-in for Rhinoceros. This plug-in allows for automatic generation of new geometries by changing certain input parameters. The model variations⁷² are then exported as a solid, using a STEP-file and imported into DIANA FEA, a finite element software.

⁷¹ A more detailed study regarding the presented numerical model can be found in (Jacobs 2017). The numerical model has been developed for type B block but corresponds to both types, since Type B block is generated by multiplying Type A. It is expected that compared to type B, type A blocks will present a slight decrease in load capacity due to extra eccentricity in loading.

⁷² Form deviations due to fabrication tolerances in the size of the unit were not considered in the final model.

Due to the fact that glass is a brittle material with a stated compressive strength approximately ten times its tensile strength, its failure behaviour cannot be described by a single-property criteria such as Von Mises stresses, which do not distinguish the value between compression and tension strength and implies a ductile behaviour. Thus, the variation models are evaluated applying the Christensen's failure criterion, which essentially converts the principal stresses and its material properties into a failure envelope definition, including a limitation for the tensile capacity of brittle materials (Christensen 2013). The criterion is given in equation 8.1:

$$\left(\frac{1}{T} - \frac{1}{C}\right) (\sigma_1 + \sigma_2 + \sigma_3) + \frac{1}{2TC} [(\sigma_1 - \sigma_2)^2 + (\sigma_2 - \sigma_3)^2 + (\sigma_3 - \sigma_1)^2] \leq 1$$

EQUATION 8.1

In which, $\sigma_1, \sigma_2, \sigma_3$ are the principal stresses, T is the tensile strength and C is the compressive strength.

The criterion includes extra conditions for brittle materials, which occur when $T/C \leq 1/2$. These conditions are given in equation 8.2.

$$\begin{aligned} \sigma_1 &\leq T \\ \sigma_2 &\leq T \\ \sigma_3 &\leq T \end{aligned}$$

EQUATION 8.2

According to (Christensen 2013) glass presents a ratio between tensile and compressive strength of approx. $T/C = 1/8$. Hence, the criterion can be used to predict at which point of the geometry tensile surface stresses become critical and can lead to failure by activating flaws. Accordingly, by loading the interlocking brickwork in shear, the generated contour plots show directly how tensile peak stresses are spread on the contact surface (Fig. 8.35). Essentially, these contour plots can be used to indicate:

- 1 where flaws in the geometry would be most influential (tensile opening of cracks)
- 2 how stress concentrations spread across the contact surface
- 3 the stress gradient at sections in the geometry

By evaluating both the contour plots and the shear lock capacity multiple geometry variations can be evaluated on their applicability as cast glass interlocking

components. The numerical model showed that any compressive load puts the geometry in a compressive state and hence yields higher shear capacities compared to when no compressive force is applied. Hence all variants were tested without any compressive load; instead the shear-load-inducing bricks were constrained in the global z-direction.

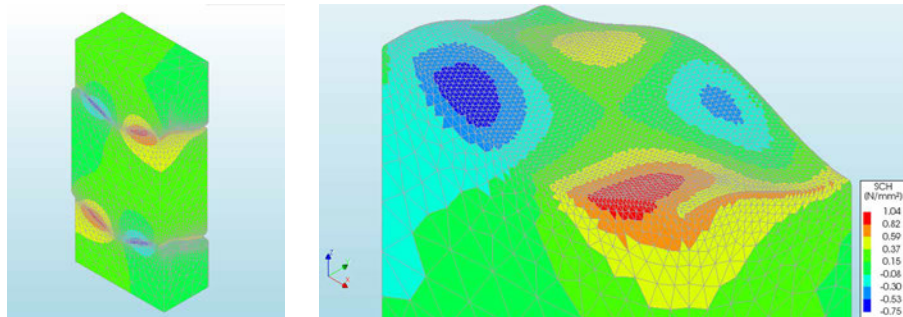


FIG. 8.35 Left: Numerical set up and results for Christensen's failure criterion value of one (SCH=1) of the tested variants. Right: Christensen's output (SCH=1) of middle brick (amplitude 10 mm). Shear capacity at failure is approximately 155 kN. Source:(Jacobs 2017).

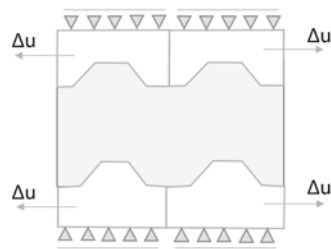


FIG. 8.36 (left) 2D Full scale principle of the model. Source:(Jacobs 2017).

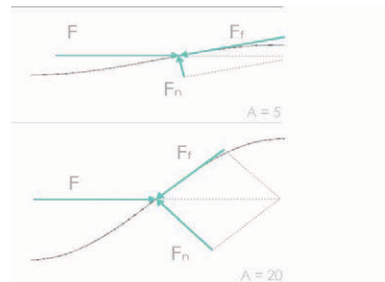


FIG. 8.37 (right) Uplifting principle for interlocking blocks with $A=5$ mm and $A=20$ mm. The shear force is depicted as a concentrated force (F) halfway the amplitude. Dead weight and weight of upper structure are not accounted for. The force is conveyed in an uplifting force (F_f) by traction tangent to the steepness at that point and in a force (F_n) by compression normal to the geometry. Source:(Jacobs 2017).

Geometry set-up

Considering the symmetry of the Type B brick design the whole model can be reduced to a quarter of its original size. This leads to fewer elements and a more efficient calculation time. Thus, to simulate a shear test, one quarter of a Type B

brick (equivalent to a full type A brick) is held between two one-eighth Type B bricks (equivalent to two halves type A bricks); in-between the glass elements two 4 mm thick PU interlayers are placed (Jacobs 2017). Fig. 8.36 shows a full-scale principle of the DIANA model in 2D.

Material settings

The input properties can be found in Tables 8.7 and 8.8 as established by (Jacobs 2017). As discussed in chapter 7.6, in general the Shore durometer scale is used to define the hardness and resistance to indentation of elastomer (and plastic) materials such as the applied PU interlayer. In theory the hardness of a polymer in a given thickness can be converted to a Young's Modulus value when in compression, as described by (Kunz, Studer 2006). Based on their experimental work on 6mm thick interlayers, the following formula for calculating the Young's Modulus of 6mm thick PU in compression is derived:

$$E_{PU;c\ 6mm} = \frac{1-\nu^2}{2RC_3} * \frac{c_1+c_2*Sh_A}{100-Sh_A} * (2.6 - 0.02 Sh_A) \quad [MPa] \quad \text{EQUATION 8.3}$$

In which $E_{PU;c\ 6mm}$ is the Young's Modulus of a 6mm thick PU in compression [MPa], ν is the Poisson's ratio, Sh_A is the Shore A hardness. R , C_1 , C_2 and C_3 are constants derived from the experimental set-up by (Kunz, Studer 2006) and have the following values:

$R = 0.395$ mm, $C_1 = 0.549$ N, $C_2 = 0.07516$ N and $C_3 = 0.025$ mm. Minor effects of friction and deviation from the ideal Poisson's value ($\nu = 0.50$) can be considered negligible. However, this formula was only validated for 6 mm polymer interlayers; there is no factor in the equation that concerns the thickness of the interlayer and no tests were performed in polymers of smaller thicknesses.

TABLE 8.7 Input properties of glass and polyurethane interlayer

Material	Glass	Polyurethane
Density	2.5*10 ⁻⁹ t/mm ³	1.1*10 ⁻⁹ t/mm ³
Poisson's ratio	0.22	0.48
Young's Modulus	70000 N/mm ²	50 N/mm ²
Tensile Strength	45 N/mm ²	-
Compressive Strength*	360 N/mm ²	-

* For the tensile strength (T) of glass the characteristic strength of annealed float glass is used. Christensen states that $T/C = 1/8$ for glass, thus, its compressive strength (C) is set to 360 MPa. In reality the compressive strength of glass can be significantly higher, but to satisfy the Christensen criterion the earlier mentioned value is applied in the model. As the leading fracture mechanism in glass occurs only due to tensile peak stresses it is not necessary to excessively review the influence of compressive stresses on the geometry.

TABLE 8.8 Input properties of interface elements

Parameter	Value	Unit
Cohesion c	0.001	N/mm ²
Normal stiffness modulus z	70 *10 ⁶	N/mm ³
Shear stiffness modulus x	7 *10 ⁶	N/mm ³
Shear stiffness modulus y	7 *10 ⁶	N/mm ³
Tensile strength gap criterion f _t	0.0005	N/mm ²
Friction angle φ	1.1	rad
Dilatancy angle	0	rad
Interface opening model	Gapping model	-

Thus, for the numerical model, the values for Poisson's ratio and Young's modulus used are calibrated using the experimental results of (Aurik et al. 2018) for PU70 interlayers of 1, 2, 3 and 4 mm thickness tested in compression. Hence the applied values are only valid for a PU with a hardness of 70A. A detailed explanation of the calibration method can be found in (Jacobs 2017). To calibrate the Young's modulus of PU to a realistic value, part of the test set up discussed in (Aurik 2017) is modelled in DIANA FEA by (Jacobs 2017). A fine mesh with element size of 2 mm is applied on the PU interlayer, and to limit calculation time and file size the mesh size is gradually increased to 20 mm. A compressive distributed load of 10.88 MPa is applied on the top glass face to conform the test setup discussed in (Aurik 2017). The Young's modulus is then varied until a deformation of 0.13 mm is found, corresponding to the result of the laboratory test. The results suggested a value of $E=50$ MPa with a Poisson's ratio equal to $\nu=0.48$ (Jacobs 2017).

Support conditions

A scheme of the support conditions can be seen in Fig. 8.38. The main object of the model is to calculate the shear capacity of the interlocking geometry. The most critical brick is expected to be at the top of the construction, where the least vertical loading is applied. Thus, one desired result of the model is to define the force necessary to prevent uplifting. Fig. 8.37 shows the principle of uplifting in the studied geometry.

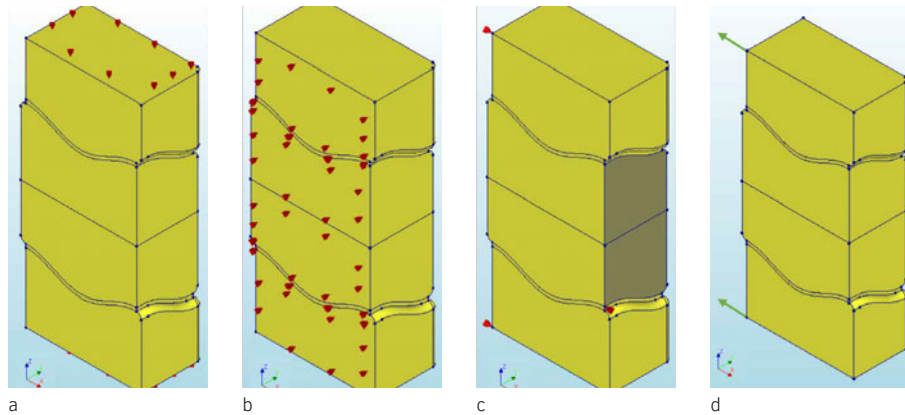


FIG. 8.38 Support conditions in a) Z-direction, b) Y-direction and c) X-direction. d) Tied vertices loaded with a prescribed deformation load. Source: (Jacobs 2017)

To evaluate the uplifting behaviour, the upper and bottom plane of the assembly are restraint in the Z direction. Due to the shear loading it is expected that parts of the geometry will tend to move upward, creating reaction forces across the planes. To simulate the symmetric geometry of the type B block, supports are added in the Y-direction. The sliced face is thus restrained in the Y-direction. In the X-direction, a similar support is needed for the middle block. One vertex is supported here which is tied to shaded faces. In this way, any deformation set in any node of these faces will have the same deformation as the master node. All reaction forces are summed into this master node, which enables easy access to the desired value of the characteristic shear strength of the geometry. Two more supports are added in the X-direction for the top and bottom bricks, to accommodate the prescribed deformation loads that introduce the desired shear loading of the assembly. Again the nodes are tied to the future mesh nodes on the corresponding surface, gaining supports and the same prescribed deformation (Jacobs 2017).

Loading conditions

As previously mentioned, a prescribed deformation is applied to the top and bottom blocks. Owing to the sliding support on top and bottom, these geometries are free to move, with only the interlocking geometry as obstacle. The applied load is conveyed through the PU interlayer to the middle block, which will in turn display the resulting stress concentrations according to Christensen's failure criterion. The load is applied on the supported vertexes, which due to the tying will copy the same deformation to any of the nodes on the tied surface. A prescribed deformation of $\Delta u = -0.1$ mm is applied to both vertexes (Fig. 8.38d) (Jacobs 2017).

Parameter ranges tested

A selection of models with different amplitude and height variants are generated and tested in DIANA. The initial model is set with an amplitude of 10 mm and a height of 150 mm. The tested amplitudes are in a range from 5 mm to 20 mm. The parameter variations for the height are between 40 mm and 150 mm. Higher bricks than 150 mm are considered impractical in terms of installation and fabrication, as the initial brick design is already approx. 17 kg in weight (Jacobs 2017).

8.4.2 Results

Fig. 8.39 gives an overview of the influence of different amplitude and brick height variants on the shear capacity.

Fig. 8.40 demonstrates that a higher amplitude would increase the shear capacity due to a larger contact area for the stresses to be distributed, while reducing the relative uplifting tendency. This is in line with the findings of the shear experiments described in section 8.3.4. A higher amplitude would also increase the chances of a shear-key failure, which is considered beneficial as it provides a warning failure mechanism. As can be depicted from the contour plots in Fig. 8.41, the tensile and compression areas grow in horizontal direction in the shear keys. This increases the probability of a shear key failure instead of a splitting brick failure. A negative effect of an increase in amplitude is that a higher precision of the brick geometry is required, as the failure limit is reached at a smaller deformation (Fig. 8.39). A

deviation from the perfect geometry⁷³ would hence lead to earlier failure for brittle materials (as also discussed by (Dyskin et al. 2003) compared to lower amplitude variations. An excessively small amplitude however would result in uplifting to become a crucial factor, needing a heavier top constraint and relying more on friction than on the interlocking geometry (Jacobs 2017). This was evident as well by the shear experiments: the osteomorphic blocks with the smallest amplitude (10 mm) would essentially slide out in a set-up of low pre-compression. The choice for a higher amplitude is therefore considered a trade-off between a higher shear capacity and a reduction in uplifting behaviour on the one hand, and geometry manufacturing precision on the other hand.

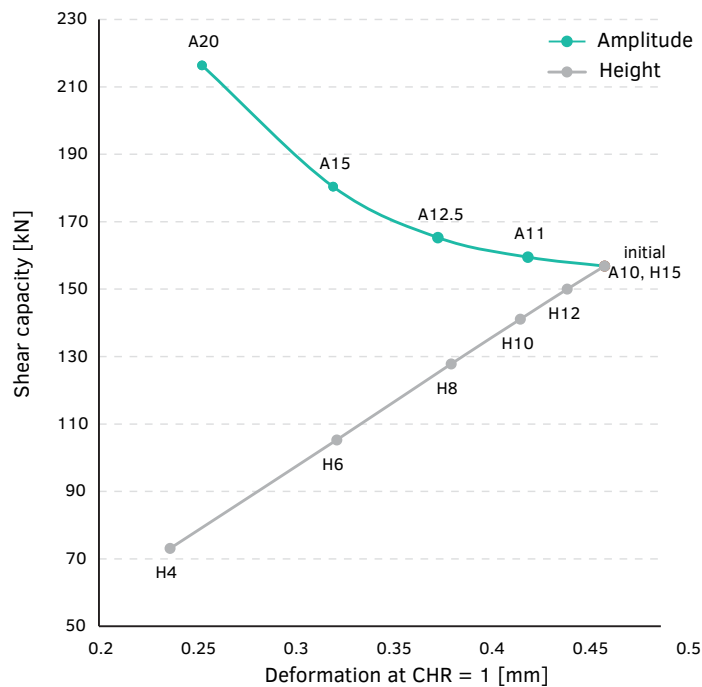


FIG. 8.39 Shear capacity and deformation at failure of the different variants. Source: (Jacobs 2017)

⁷³ As a reference, in current adhesively-bonded cast glass applications, cast glass blocks are made with fabrication tolerances ranging between ± 0.25 mm (Oikonomopoulou et al. 2015b) to ± 1.00 mm (Goppert et al. 2008).

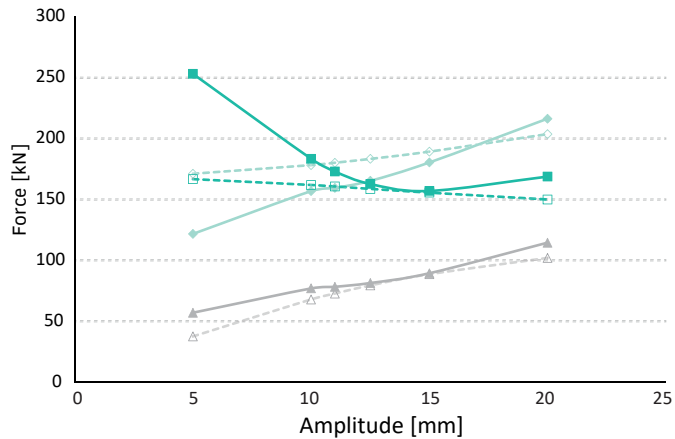


FIG. 8.40 Influence of amplitude on shear capacity, uplifting force (parallel to interlock curvature) and reaction forces. The prediction lines are based on hand calculations described in (Jacobs 2017).

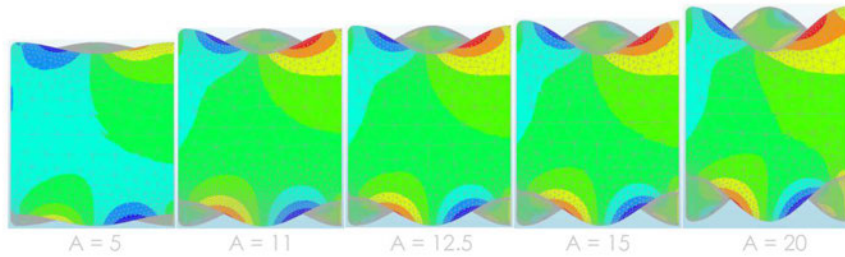


FIG. 8.41 Contour plots at failure load for various amplitude variations, demonstrating the stress redistribution of the given geometries. For the failure loads of each amplitude variation refer to Fig. 8.39. Source: (Jacobs 2017)

Fig. 8.42 exhibits the influence of the height of the brick on the failure mode of the glass brick. The graph suggests that failure through bending is critical in lower brick heights (in this case less than 80 mm in height) as they are subject to higher stresses due to eccentric loads. Higher variants are more resistant to this, leading to shear key failure. These failure mechanisms are expected to occur in the most flaw-prone area, as derived from the Christensen's failure criterion. Thus, the upper boundaries were determined from a simplified hand calculation, described in (Jacobs 2017), using the characteristic strength of glass. It is expected that the real value is to a certain degree lower, as the combination of the principal stresses in the

Christensen's criterion lead to failure before this characteristic value is reached. Thus, Fig. 8.42 incorporates the results from the finite element analysis versus the simplified hand calculations. Regarding geometry tolerances, higher bricks are also advantageous, as the failure load occurs at a larger deformation. This means a larger geometry deviation is allowable when producing higher bricks compared to shorter bricks. Therefore, a higher brick is beneficial for brick design, as load capacity is increased, tolerances can be slightly higher and there is an increased probability for the preferred failure mechanism: an interlock chipping off would leave the remainder of the component intact, maintaining thus to a certain extent the structural integrity of the unit.

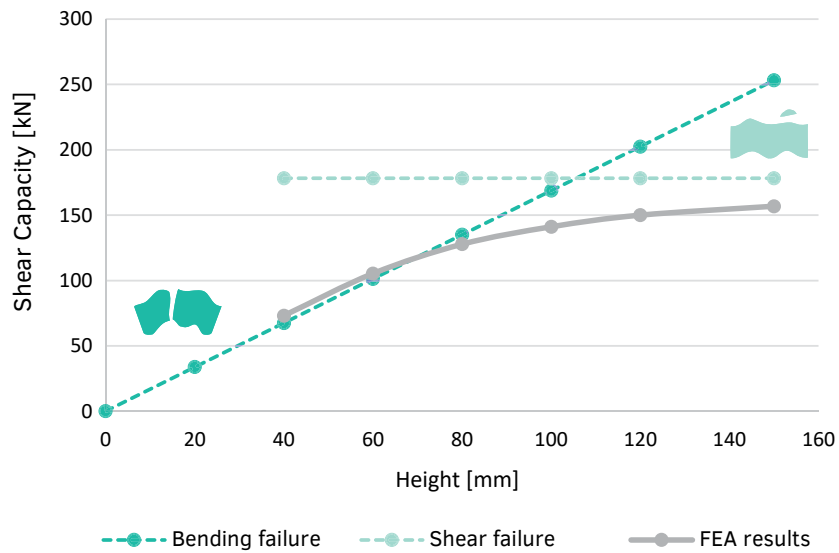


FIG. 8.42 The effect of the height on the shear capacity of the brick plotted together with the expectations from hand calculations. Source: (Jacobs 2017).

8.5 Conclusions

In this chapter, the experimental and numerical investigation of a dry-assembly system out of interlocking solid cast glass blocks has been presented in order to investigate the influence of various parameters in the overall performance of the system. The main parameters that are investigated are the amplitude and height of the interlocking blocks and the thickness and Shore Hardness of the interlayer.

8.5.1 Conclusions from the interlayer testing under static load

As discussed in Chapter 7, the use of a dry interlayer is essential for evenly distributing the stresses between the blocks and preventing direct contact between the glass elements. Thus, a selection of interlayers with a Shore Hardness between 60A – 80A and a thickness of 3 or 6 mm were tested under static creep at a 40kN compressive load for 900 s, corresponding to a nominal compressive stress of approx. 14.2 MPa. It should be noted that the applied load is considered very strict – in a real application a considerably less nominal compressive stress is anticipated.

Each interlayer was cast in the desired shape, matching the interlocking geometry of the blocks and tested between two half osteomorphic cast glass blocks. The results highlighted that the tear strength of the interlayer is equally important to its Shore Hardness. Interlayers with a relatively low tear strength will fail due to the tearing of the interlayer, leading to the direct contact of the glass blocks which in turn results in concentrated stresses and local failure. It was also concluded that harder interlayers, e.g. with a Shore Hardness between 70A and 80A are the most promising candidates for the realization of the examined system; they can withstand the anticipated compressive static loads with little or no plastic deformation. Nonetheless, experiments on higher loads suggested that the lateral deformation of the interlayer due to creep in combination with high manufacturing tolerances can lead to the eventual failure of the glass blocks due to peak stresses. Further research is thus necessary in order to find a transparent interlayer that presents a time-independent behaviour under static compressive load. The testing under static load of glass block assemblies with different interlayers indicated that 6mm interlayers behave stiffer than the 3 mm variant for the given interlocking geometry and manufacturing tolerances. The increased stiffness can be attributed to the increased contact achieved by the thicker interlayer. Nonetheless, it should be noted that although the interlayer itself becomes stiffer when thicker, the stiffness of the overall assembly

is actually compromised (and the risk for buckling is thus increased), as discussed in Chapter 7. Thus, an interlayer of the minimum required thickness for full contact between the blocks is recommended. In our case, due to the manual fabrication and post-processing of the blocks, it was determined to proceed with 6 mm thick interlayers for the further experimental investigation of the system in out-of-plane shear. In a real application though, where the high manufacturing accuracy of the blocks is presumed, interlayers 3 mm thick should suffice for accommodating the dimensional discrepancies, providing a higher overall stiffness. Lastly, this series of tests highlighted that the geometry of the interlocking system is equally as, or even more critical to the interlayer used. As the experiments demonstrated sharp changes of curvature, such as the ones at the edges of the interlocking system, can lead to the local perforation of (some of) the interlayers and in turn to the early failure of the assembly due to glass-to-glass contact. Thus, smoother curvature changes along the interlocking surfaces are preferred.

Another conclusion regarding the interlocking geometry derived from this series of tests is that the more pronounced the amplitude of the interlocking system, the more prone is the assembly to manufacturing intolerances and thus to the introduction of concentrated tensile stresses because of insufficient contact (mismatch) and collaboration between the interlayer and the glass units. This can be improved either by introducing a thicker interlayer, which however would further compromise the stiffness of the assembly, or by a smoother interlocking mechanism with reduced wave amplitude.

8.5.2 **Conclusions from the out-of-plane shear testing of assemblies with various amplitudes**

In this series, assemblies of 3 osteomorphic blocks, with various amplitudes, namely 10, 15 and 20 mm were tested in series of 3 specimens each under increasing load in out-of-plane shear. Overall, the results indicated that assemblies out of blocks with higher amplitudes in their interlocking mechanisms behave stiffer and withstand higher loads. They also present less visible deformation, expressed as the shifting of the loaded middle block downwards, prior to failure. The findings are in line with the conclusions derived by the numerical model described in chapter 8.4.

All specimens - with the exception of the specimens with 10 mm amplitude that reached the max. set deformation without cracking - failed initially at the middle glass block. The latter, prior to cracking, shifted visibly downwards; as the assembly is free to rotate under bending. The only resistance to the bending moment is

provided by the peripheral constraining force, which in this case was considerably low. This in turn results to a limited load-bearing capacity of the system prior to failure. In particular, the middle block consistently got fractured at the point where the interlocking curvature was changing from concave to convex. There was no crack propagation occurring at any of the assemblies – cracks at the adjacent blocks occurred non-simultaneously and at different locations, validating the assumption that the assembly presents an increased fracture toughness. None of the specimens collapsed upon failure; the fragmented blocks were still able to carry the load.

Moreover, upon release of the load the individual blocks showed a tendency to self-align towards their initial configuration. Due to time restrictions, the amount of recovery after the load removal was not investigated in detail. Although compared to a monolithic variant the assembly is less stiff and is anticipated to fail at considerably lower stress, its increased structural safety and damage tolerance can allow the engineering of structures with a considerably lower safety factor. Firstly, the failure of the described system is localized and does not lead to global failure. Secondly, despite the lower bending stiffness of the proposed system compared to the one of a monolithic variant, the high deflection at failure allows the assembly, made of brittle components, to behave as a pseudo-ductile, as discussed in Chapter 7. This behaviour provides a warning mechanism prior to failure that increases the safety of a relevant structure.

The consistent locations of the cracks in all specimens also suggest that defects in the meso-structure (inner volume) of the blocks or in locations where peak stresses are not anticipated are not expected to be critical in the overall structural performance of an interlocking assembly. This, however, should be further investigated.

Lastly, this series of specimens highlighted that the overall stiffness of the assembly can be compromised by multiple factors that should all be considered in a real construction. These include the dimensional tolerances of the individual blocks, as well as of the entire construction. These tolerances are in turn reflected to the thickness of the employed interlayer. In principle, the thinner the interlayer, the stiffer the assembly, provided that there is complete contact achieved. As explained previously, the geometry of the interlocking mechanism further influences the stiffness. Interlocking mechanisms of higher amplitudes are in principle yielding a more stiff structure. Yet, as the experiments indicated, they are also more prone to failure due to dimensional deviations, due to the generation of peak stresses at areas of insufficient contact. Moreover, higher amplitudes are more prone to induce eccentricity in construction during assembly. An alternative solution to prevent this,

would be the design of a component with multiple interlocking mechanisms and thus, improved self-aligning capacity, such as the Type B block presented in Chapter 7.

Lastly, the amount of pre-stress employed plays a crucial role in stiffening the assembly. Higher pre-stressing can further stiffen the structure and prevent the misalignment of the blocks by the anticipated lateral loads. Yet, this presumption needs to be further investigated and validated. An additional challenge of the described dry-assembly, interlocking system anticipated in a real construction concerns the assembly, proper alignment and controlled pre-compression of such a system upon installation.

8.5.3 Conclusions from the numerical modelling

The numerical model provided valuable input regarding the influence of the geometrical parameters of the interlocking geometry in the overall structural performance in shear. In specific, it was shown that a decrease in the height of the blocks lowers their shear capacity and alters the system's failure mechanism: a lower brick is more susceptible to bending failure, whereas for higher brick variants the shear lock failure is proven to be more critical. Both failure mechanisms are nevertheless still possible, even for higher bricks, as peak tensile stresses occur at the middle of the block. The latter was confirmed as well by the first series of compressive tests on different interlayers. A flaw in that area could lead to crack propagation normal to this region. It was also demonstrated that an increased amplitude of the interlock is beneficial as it leads to an enhanced shear capacity and decreased uplifting effects, as was also suggested by the out-of-plane shear experiments. Increased amplitudes also require a higher precision in manufacturing as the components can reach the failure stress limit at considerably lower deformation.

8.6 Recommendations

Overall, a novel dry-assembly system employing interlocking solid glass blocks was introduced in the last two chapters. The numerical and experimental investigation of the proposed system offered valuable insights into the mutual influence of various

parameters on the mechanical performance; yet, it also showed that there is still a lot of room for exploration. Accordingly, in this section some possible directions for future research are briefly discussed.

Firstly, although the general principles of the osteomorphic interlocking geometry have already been experimentally investigated, the performance of the system will be further improved if smoother curvature changes are incorporated at the blocks, particularly at their edges. Smoother curvature changes reduce the risk of perforating the interlayer and together, the risk of localized stresses in these locations. Yet, smoother curvatures can also result in an interlock of lower amplitude, of reduced shear capacity and decreased uplifting resistance.

The experiments in out-of-plane shear clearly demonstrate that an assembly of the given geometry allows for significant deformation under loading. This is partially attributed to the manufacturing tolerances of the kiln-cast components that necessitated the use of thicker (6 mm) interlayers. The re-investigation of the system with components produced by hot-pouring in high accuracy steel moulds is strongly recommended. It is expected that cast glass units that are industrially manufactured will present a considerably higher degree of dimensional accuracy which in turn would not necessitate an interlayer thicker than 2-4 mm. The use of borosilicate glass can further contribute in achieving high accuracy components due to its reduced thermal expansion coefficient (and thus shrinkage during annealing)⁷⁴.

It was also shown that components with increased amplitudes in the examined osteomorphic interlocking mechanism, although able to sustain considerably higher loads, are more prone to eccentricity during assembly. To minimize the occurrence of eccentricity in a construction, the design of an interlocking geometry with more locks is recommended, such as Type B block presented in chapter 7.5.2 and used in the numerical investigation of the system. Such a geometry can present improved self-alignment properties and extra redundancy in case of failure of individual locks of the interlocking mechanism.

Further research is also necessary in order to find a transparent interlayer that presents a time-independent behaviour under long-term static load. The use of a multi-layer interlayer – with a stiffer core and softer external layers - but also the use of soft aluminium as an interlayer are recommended for future research. The most suitable thickness of the interlayer should be determined using interlocking blocks

⁷⁴ Based on the work of (Goppert et al. 2008), it is anticipated that industrially manufactured glass blocks can present a dimensional accuracy of ± 1.0 mm without any post-processing.

industrially manufactured with a higher dimensional precision. For assemblies out of interlocking blocks, the degree of self-realigning back to the initial configuration upon load release should also be documented in detail.

Due to time and financial constraints, the effect of pre-stress was not investigated in this work. The engineering of a constraining frame with a controlled pre-stressing mechanism that can further stiffen the assembly is essential for the real application of the presented system in the built environment. In this direction, future research should focus on evaluating the stiffness of the assembly based on different amounts of pre-stress. Work by (Dyskin et al. 2003) focusing on a concentrated load test on a plate-like assembly out of similar (yet smaller in scale) osteomorphic blocks made by brittle *PolyLite 61-209* resin has already indicated that the deformation behaviour and stiffness of such an assembly is strongly pressure dependant.

Moreover, an assembly method that ensures the proper alignment of the components prior, during and after the necessary pre-compression should be developed.

A detailed study on the sealing of the system against weathering and its performance under thermal fluctuations are also recommended.

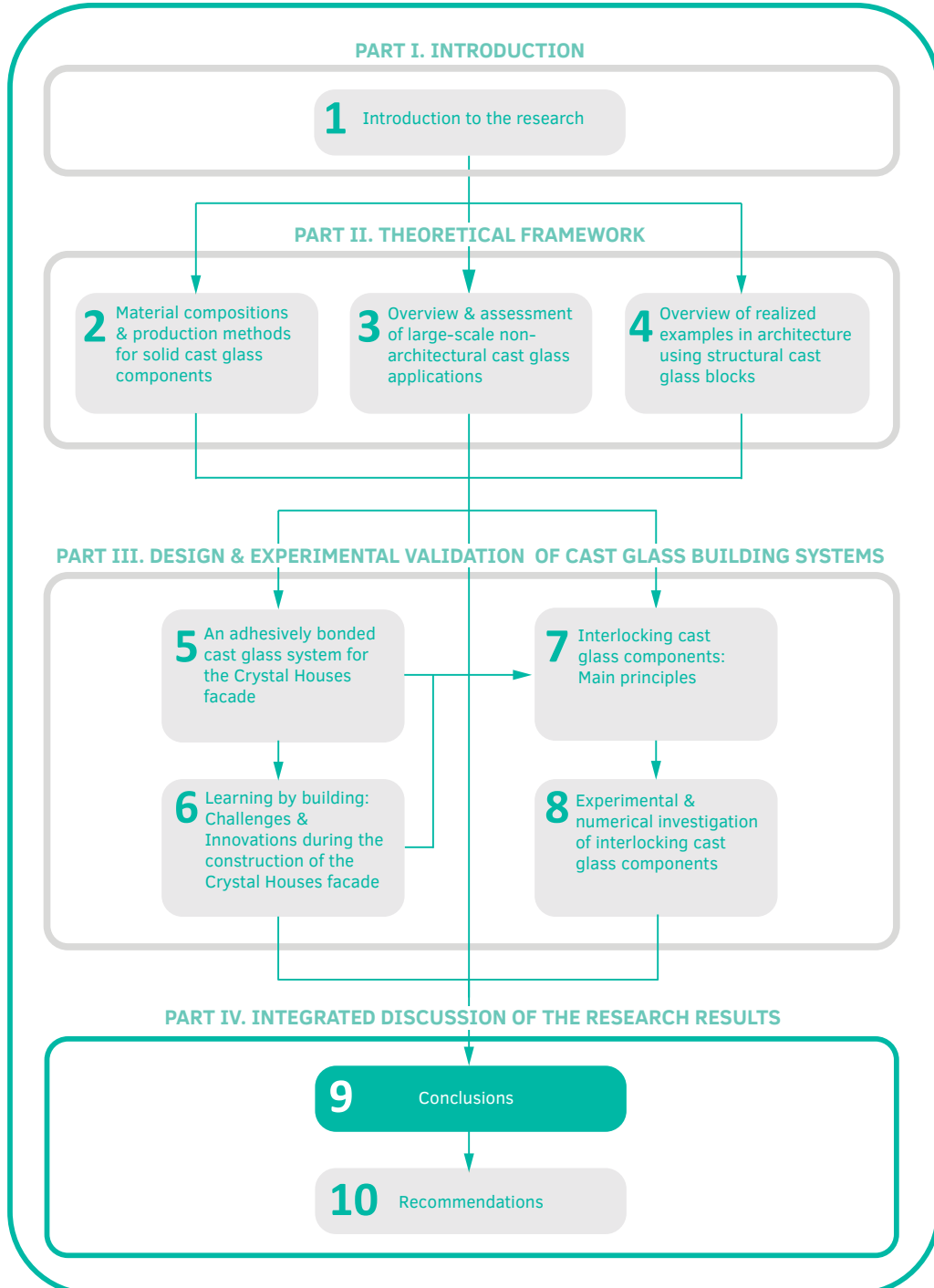
Lastly, a valuable experiment that could further quantify the properties of the proposed interlocking system is the comparison of the performance of an interlocking plate-like assembly under concentrated load to the ones of a monolithic glass plate of equivalent thickness and of a similar assembly that is adhesively bonded.



Osteomorphic cast glass blocks made of recycled CRT, art and float glass at the *Glass & Transparency Lab* of TU Delft.



Exploring the third dimension of glass



Solid cast glass components and assemblies for structural applications